Dynamic response of structures to thunderstorm outflows: response spectrum technique vs time-domain analysis

Giovanni Solari [a] *, Patrizia De Gaetano [a]

[a] *Department of Civil, Chemical and Environmental Engineering, Polytechnic School, University of Genoa, Via Montallegro 1, 16145 Genoa, Italy*

* *corresponding author*, giovanni.solari@unige.it

ABSTRACT

Thunderstorms are transient events. Design wind velocity and wind-induced damage are often related to them. Despite this, research on thunderstorm loading of structures is still fragmentary and uncertain due to their complexity, short duration and small size. These issues make it difficult to set physically realistic and simple models as well as to gather real data. This favoured the implementation of refined methods based on limited measurements. The European Projects "Wind and Ports" and "Wind, Ports and Sea" realised an extensive monitoring network from which many thunderstorm outflow records were extracted. They were analysed to inspect their characteristics and to formulate methods coherent with measurements. Firstly, the response spectrum technique conceived for earthquakes was extended to thunderstorms. Then, a hybrid simulation strategy was proposed and time-domain integrations of the structural response were applied. This paper provides a joint calibration and advancement of these two methods, leading to results that substantially agree, especially faced with their conceptual and operative diversities. This confirms the potential of the response spectrum technique to become a suitable tool for calculating the thunderstorm loading of structures and the efficiency of hybrid simulations and time-domain analyses to investigate, with a limited computational burden, advanced structural issues.

KEYWORDS

Hybrid simulation; Monitoring network; Non-stationary response; Response spectrum technique; Time-domain integration; Thunderstorm outflow.

1. INTRODUCTION

The study of thunderstorm outflows and their loading of structures is a dominant topic of modern wind engineering [1, 2]. This mainly depends on the fact that methods currently applied to determine the wind-excited response of structures are still mostly based on models related to the synoptic phenomena that evolve in about 3 days on around 1,000 kilometres on the horizontal. They give rise to nearly stationary wind fields (Fig. 1a) that occur in almost neutral atmospheric conditions, with velocity profiles in equilibrium with the atmospheric boundary layer (ABL) [3].

Thunderstorms are mesoscale atmospheric phenomena that consist of a set of cells that evolve in about 30 minutes on a few kilometres on the horizontal [4]. They give rise to intense transient downdrafts (Fig. 1b) that impact the earth's surface followed by radial outflows with a typical "nose" profile [5, 6] and horizontal ring vortices (Fig. 2). The ensemble of these air movements is called "downburst" and is divided into macroburst and microburst depending on whether its size is greater or smaller than 4 km [7]. The design wind velocity is often related to strong microbursts that may occur individually or along squall-lines. Such events are usually embedded into more or less intense background synoptic phenomena and the damage caused by wind at the mid-latitudes is often due to these situations.

Despite the extensive research carried out on thunderstorm loading and response of structures in the last decades, the knowledge of this matter is still fragmentary and full of uncertainties [2]. This depends, on the one hand, on the complexity of one of the most spectacular and impressive phenomena that nature produces, and, on the other hand, on its short duration and small size. The first issue makes it difficult the formulation of engineering models physically realistic and simple to apply as for cyclonic synoptic events [3]. The second makes the available measurements very limited.

The literature is rich in contributions to determine the dynamic response of Single-Degree-Of-Freedom (SDOF) systems, N-DOF (NDOF) systems and slender beams to thunderstorm outflows. It exhibits a wide panorama of procedures whose complexity matches the complexity of these phenomena.

This research pathway started in 2002, when Choi and Hidayat [8] studied the time-domain response of a SDOF system to thunderstorm outflows identically coherent in space, to generalize the classic gust factor technique introduced by Davenport [3] in 1961 with reference to cyclonic synoptic events. This approach was developed by Chen and Letchford (2004) [9], who analyzed a SDOF system by means of a so-called Maximum Dynamic Magnification Factor, given by the ratio between the maximum value of the dynamic response and the static response to the peak loading, by Holmes et al. (2005) [10], who used Duhamel's integral to calculate the response of structures to thunderstorm winds, and by Chay et

al. (2006) [11], who applied a time-domain approach based on ARMA simulations. Chen (2008) [12] studied the dynamic response of a building to a transient wind field modelled by an evolutionary power spectral density (EPSD). Kwon and Kareem (2009) [13] proposed a gust front factor framework where the original gust response factor technique [3] was generalized from stationary to non-stationary wind actions by an EPSD approach. Le and Caracoglia (2015) [14] used the Wavelet-Galerkin method to evaluate the non-linear and/or non-stationary response of SDOF and NDOF systems. They also proposed (2018) [15] a computer model of the transient dynamic response of a tall building subjected to a digitally simulated thunderstorm wind field coherent with an EPSD representation.

Many other papers did not reach the evaluation of the wind-induced response, but provided propaedeutic methods to represent transient wind fields. For instance, Wang et al. (2013) [16] conceived a data-driven approach to simulate full-scale downburst wind speeds by Hilbert transform, stationary wavelet transform, and Proper Orthogonal Decomposition (POD). Huang et al. (2015) [17] applied the discrete wavelet transform and the kernel regression method to infer the time-varying mean and variance of non-stationary extreme wind speeds, respectively; then, based on the estimated EPSD, they examined the transient features of non-stationary winds. Peng et al. (2017) [18] simulated multi-variate non-stationary wind fields along lines with uniformly distributed nodes, based on the application of hybrid stochastic waves and POD factorization.

A dominant aspect of most of these contributions is the striking contrast between the formulation of highly refined advanced procedures and the poorness of the experimental measurements used to support theory. In some cases authors acknowledge that methods proposed are theoretical models waiting for real data to make them explicit. In other cases the formulations and applications are based on an inadequate number of measurements in order to ensure the robustness and physical sense of analyses. Sometimes, the use of sophisticated methods faced with the almost total lack of data seems to be quite questionable, especially when analyses are carried out in a probabilistic framework.

The European Projects “Wind and Ports” [19] and “Wind, Ports and Sea” [20] offered authors and the Windyn Research Group (www.windyn.org) a unique opportunity to follow a different pathway according to which novel methods robustly coherent with real data have been formulated for determining the wind-induced response of structures to transient thunderstorm outflows.

In this framework, an extensive wind monitoring network has been created in the High Tyrrhenian area, from which many records of thunderstorm outflows have been extracted [21]. Such records have been

analysed first aiming to evaluate their statistical properties [22], then to develop consistent methods to determine the wind loading and response of structures. Firstly, the response spectrum technique widely used in the seismic field [23] and introduced in [24] for synoptic winds was generalised to thunderstorm outflows [25, 26]. Then, a hybrid strategy to simulate transient wind velocity fields of thunderstorm outflows was developed and time-domain integrations of the wind-induced response of slender vertical structures were carried out [27].

This paper recalls these two methods, compares them critically, examines their own merits and defects, develops a parallel application and joint calibration assessment that improve their comprehension and accuracy, leading to results that substantially agree, especially considering conceptual and operative diversities, faced with the complexity of the exciting phenomenon. This confirms, on the one hand, the potential of the response spectrum technique to become a suitable engineering tool for calculating the thunderstorm loading of structures, and, on the other hand, the high efficiency of hybrid simulations and TDA to investigate, with a limited computational burden, advanced issues such as the multi-modal response and the non-linear behaviour of structures.

Section 2 describes three real structures [27] used as reference test cases throughout this paper. Section 3 summarizes the thunderstorm outflow velocity model on which the time-domain analysis (TDA) [27] and the thunderstorm response spectrum technique (TRST) [26] are based. Section 4 illustrates the hybrid strategy to simulate thunderstorm outflow velocity fields [27], determines the time-domain response of the structure test cases in Section 2, and extracts the probability density function (PDF) of the maximum value of their top displacements. Section 5 recalls the Equivalent Wind Spectrum Technique (EWST) [28, 29], its generalization from stationary to transient wind fields [26], and the advantages involved by embedding this method into the hybrid simulation strategy. Section 6 recalls and up-grades TRST [26, 27]. Section 7 compares TRST and TDA, discusses their merits and defects, points out their agreement with regard to the mean value of the maximum response, highlights and interprets the disagreement concerning the spread of results. Session 8 develops an alternative formulation of TRST [26] that reduces the spread of results, without compromising the quality of the mean values. Section 9 introduces a probabilistic assessment of TRST that further reduces the above spread. The improved agreement between TRST and TDA obtained in Sections 8 and 9 proves their parallelism but is pursued at the expense of a more efficient and/or simple use of the TRST. Section 10 summarizes the main conclusions and draws some prospects for future research.

2. STRUCTURE TEST CASES

Three real slender vertical structures were examined as reference test cases: a steel lighting pole, a steel telecommunication antenna mast and a reinforced concrete telecommunication tower. They correspond to the structure test cases already analysed in [27]. Differently from that paper, however, two values of the damping coefficient are investigated: the first one, ξ_a, is the same adopted in [27]; the second, ξ_b, corresponds to a lower damping value aiming to amplify the resonant part of the response and to test the efficacy of the proposed methods in extreme conditions.

The steel lighting pole (S1) is made up of a shaft and a top lighting device. The shaft consists of two parts with truncated conical shape and tubular octagon section with a constant thickness of 4 mm. Its height above the ground level is 14 m, of which 2.2 m correspond to the lower part and 11.8 m to the upper one. The outer base and top diameters are 280 and 80 mm, respectively. The lighting device has a mass of 145 kg with a barycentre at 14.9 m height. The total height of the pole is 15.76 m.

The steel telecommunication antenna mast (S2) is made up of two shafts with tubular circular section and a total height of 36 m. The lower shaft, referred to as the main one, is 30 m long and consists of 5 parts, each one 6 m long, with constant outer diameters 914.8, 812.8, 711.2, 609.6, 508.0 mm and thicknesses 8.0, 8.0, 7.1, 6.3, 5.6 mm, respectively. The upper shaft is 6 m long; its cross-section has a constant outer diameter of 193.7 mm and a thickness of 7.1 mm; it may carry up to 6 antennas that are not installed in the present arrangement.

The reinforced concrete telecommunication tower (S3) is made up of 3 superimposed shafts. The lower shaft, up to 3.90 m height, consists of two concentric tubular circular sections linked by 6 radial walls. The intermediate main shaft, from 3.90 to 80.50 m, has circular tubular section with outer diameter of 6.50 m and thickness of 0.50 m; in its upper part, from 59.50 to 80.50 m, there are 7 steel platforms, with constant distance 3.50 m, that carry transmission parabolic dishes. The upper shaft, from 80.50 to 98.00 m, has circular tubular section with outer diameter 3.00 m and thickness 0.25 m; its outer surface carries 4 tubular steel uprights that support other parabolic dishes. Inside the tower there is a staircase and an elevator that stops at 80.50 m height.

For each structure, Fig. 3 shows a picture, the model scheme, and the first 3 modal shapes ψ_1, ψ_2, ψ_3. Table 1 provides the main properties: H is the total height; n_1, n_2, n_3 are the first 3 natural frequencies; ξ_a, ξ_b are two structural damping coefficients; N is the number of nodes of the structural model.

3. WIND VELOCITY MODEL

Both TDA [27] and TRST [26] are based on the wind velocity model described and discussed in [26, 27]. Its main features are reported below for the sake of completeness.

The horizontal component of the wind velocity in a thunderstorm outflow (Fig. 1) along a vertical axis is expressed by the classical decomposition rules [30, 31]:

$$v(z,t) = \overline{v}(z,t) + v'(z,t) \tag{1}$$

$$v'(z,t) = \sigma_v(z,t)\,\tilde{v}'(z,t) \tag{2}$$

where z is the height above ground, $t \in [0, \Delta T]$ is the time, $\Delta T = 10$ minutes, $\overline{v}$ is the slowly-varying mean wind velocity, v' is the residual fluctuation, σ_v is the slowly-varying standard deviation of v', $\tilde{v}'$ is the reduced turbulent fluctuation dealt with as a stationary Gaussian random field with zero mean and unit standard deviation. The extraction of $\overline{v}$ from v and of σ_v from v' is carried out by a moving average filter with a moving average period T = 30 s [22, 31]. Replacing Eq. (2) into Eq. (1) the wind velocity is given by:

$$v(z,t) = \overline{v}(z,t)\left[1 + I_v(z,t)\,\tilde{v}'(z,t)\right] \tag{3}$$

where I_v is referred to as the slowly-varying turbulence intensity:

$$I_v(z,t) = \frac{\sigma_v(z,t)}{\overline{v}(z,t)} \tag{4}$$

The decoupling of space and time in $\overline{v}$ and I_v allows us to express these two quantities as:

$$\overline{v}(z,t) = \overline{v}_{max}(h)\,\alpha(z)\,\gamma(t) \tag{5}$$

$$I_v(z,t) = \overline{I}_v(h)\,\beta(z)\,\mu(t) \tag{6}$$

where $\overline{v}_{max}$ is the maximum value of $\overline{v}$ in ΔT; h is the reference height of the wind velocity; α is a non-dimensional function of z that defines the shape of the vertical profile of $\overline{v}$ [32-36], being $\alpha(h)=1$; γ is a non-dimensional function of t that expresses the time variation of $\overline{v}$ [22, 37], being $\gamma_{max}=1$. Similarly, $\overline{I}_v$ is the average value of I_v in ΔT; β is a non-dimensional function of z that defines the shape of the vertical profile of $\overline{I}_v$ [13, 22], being $\beta(h)=1$; μ is a non-dimensional function of t that expresses the time variation of I_v [22], being $\overline{\mu}=1$.

The reduced turbulent fluctuation $\tilde{v}'$ is identified through its cross-power spectral density (CPSD):

$$S_{\tilde{v}'\tilde{v}'}(z,z',n)=\sqrt{S_{\tilde{v}'}(z,n)\,S_{\tilde{v}'}(z',n)}\,Coh_{\tilde{v}'\tilde{v}'}(z,z',n) \tag{7}$$

z' being a height above ground, n the frequency, $S_{\tilde{v}'}$ and $Coh_{\tilde{v}'\tilde{v}'}$ the PSD and the coherence function of $\tilde{v}'$, respectively. These quantities are expressed here by the classical models for synoptic winds [38]. Replacing Eqs. (5) and (6) into Eq. (3), the wind velocity is given by:

$$v(z,t)=\overline{v}_{max}(h)\alpha(z)\gamma(t)\left[1+\overline{I}_v(h)\beta(z)\mu(t)\tilde{v}'(z,t)\right] \tag{8}$$

Finally, the peak wind velocity is defined here as the maximum value of v averaged in a time interval $\tau \ll \Delta T$, being $\tau=1$ s. It is given by the relationship [30]:

$$\hat{v}(z)=\overline{v}_{max}(z)G_v(z)=\hat{v}(h)\alpha(z) \tag{9}$$

where $G_v=\hat{v}/\overline{v}_{max}$ is the velocity gust factor assumed here as independent of z [22].

4. TIME-DOMAIN ANALYSIS

TDA consists of two steps: the simulation of the wind velocity field (Section 4.1) and the integration of the equations of motion (Section 4.2).

4.1. Hybrid Simulation

Diversely from classical Monte Carlo simulations of non-stationary vector fields [39-44] and from some techniques recently developed for downbursts [16, 18], the hybrid strategy proposed in [27] to generate artificial velocity fields of thunderstorm outflows is aiming to capture their inherent properties by making recourse to simple physical concepts and real velocity records. This strategy is based on assembling the different ingredients that make up the wind velocity model in Eq. (8), taking into account their sources of randomness in an appropriate way and with high computational efficiency. Table 2 lists the 5 steps of this procedure. A brief description of each step is given below.

Step 1: Velocity scaling. Although the limited number of measured thunderstorm outflows makes it difficult to determine suitable distributions of their extreme wind speed, this is a key issue. According to preliminary estimates, in [26, 27] the maximum value of $\overline{v}$ at h = 13 m with 50 years return period was assigned as $\overline{v}_{max}$ = 36.5 m/s.

Step 2: Vertical profiles. Modelling the vertical profiles of $\overline{v}$ and I_v by $\alpha(z)$ and $\beta(z)$, respectively, is another key issue for the persistent lack of measured data along vertical axes. The uncertainties in the profile of $\overline{v}$ were taken into account by varying parametrically the parameters of a suitable theoretical model of $\alpha(z)$. In [26, 27] the model proposed in [34] was adopted and $J = 4$ values z_m = $25,50,75,100$ m of the height at which $\overline{v}$ is maximum were selected. As for the vertical profile of I_v, $\beta(z) = 1$ was used [26, 27].

Step 3: Slowly-varying time dependence. The random time-dependence of $\overline{v}$ and I_v was simulated by gathering $K = 93$ thunderstorm outflow records [22] and extracting from them synchronous pairs of $\gamma(t)$ and $I_v(z,t) = I_v(h,t) = \overline{I}_v(h)\mu(t)$ sample functions (Eqs. (5) and (6)).

Step 4: Turbulence field. The randomness of the space-time variation of the stationary Gaussian field $\tilde{v}'$ was simulated by a Monte Carlo algorithm [45] based on spectral representation [46, 47]. Its computational efficiency was increased by substituting harmonic superimposition by a Fast Fourier Transform based implementation [48] and by factorizing the PSD matrix of $\tilde{v}'$ by its POD eigenvalues and eigenvectors [49, 50]. The PSD and the coherence function of $\tilde{v}'$ were expressed by [38]:

$$S_{\tilde{v}'}(z,n) = \frac{6.868 L_v(z)/\overline{v}_{max}(z)}{\left[1+10.302 n L_v(z)/\overline{v}_{max}(z)\right]^{5/3}} \tag{10}$$

$$Coh_{\tilde{v}'\tilde{v}'}(z,z',n) = exp\left\{-\frac{2nc_z|z-z'|}{\overline{v}_{max}(z)+\overline{v}_{max}(z')}\right\} \tag{11}$$

where $L_v(z) = 34.6$ m is the average integral length scale of $\tilde{v}'$ evaluated in [22] and $c_z = 10$ is the exponential decay coefficient of $\tilde{v}'$ along z classically assigned to longitudinal turbulence in synoptic winds [38]. The identification of the slowly-varying mean wind velocity $\overline{v}$ with its maximum value $\overline{v}_{max}$, though common in literature, calls for better investigations. Coherently with measurements, simulations were carried out with a time step Δt = 0.1 s in a time interval ΔT = 10 minutes. The turbulence harmonic content was simulated between 0 and the cut-off frequency n_c = 5 Hz, with a frequency resolution $\Delta n = 1/600$ Hz. $L = 1{,}000$ artificial wind fields of $\tilde{v}'$ were simulated for each $J = 4$ velocity profiles.

Step 5: Component assemblage. $M = J \times K \times L = 4 \times 93 \times 1{,}000 = 372{,}000$ thunderstorm velocity fields were simulated for each of the 3 test structures examined. Since they are discretized by $N = 16, 19, 26$ joints (Table 1), all in all 22,692,000 artificial velocity histories were generated. Fig. 4 shows 3 sample functions of a wind velocity field with $z_m = 50$ m.

The performance of the whole simulation algorithm was discussed in [27], where it was shown that the hybrid technique compared with target requirements is endowed with limited errors and produces wind fields adhering to measured data.

4.2. Integration of the Equations of Motion

Coherently with the formulations developed in [26, 27], let us consider a slender vertical structure with linear elastic behaviour. Using modal analysis, assuming that natural frequencies are well-separated and dealing with damping as small and proportional, its dynamic alongwind displacement is given by:

$$x(z,t) = \sum_k \psi_k(z)\, p_k(t) \tag{12}$$

where ψ_k is the k-th mode shape and p_k is the k-th principal coordinate:

$$\ddot{p}_k(t) + 2\xi(2\pi n_k)\dot{p}_k(t) + (2\pi n_k)^2 p_k(t) = \frac{1}{m_k} f_k(t) \tag{13}$$

m_k and f_k being the k-th modal mass and modal force, respectively:

$$m_k = \int_0^H m(z)\psi_k^2(z)\,dz \tag{14}$$

$$f_k(t) = \int_0^H f(z,t)\psi_k(z)\,dz \tag{15}$$

in which m is the structural mass per unit length and f is the aerodynamic wind loading:

$$f(z,t) = \frac{1}{2}\rho v^2(z,t) b(z) c_D(z) \tag{16}$$

ρ is air density, v is the wind velocity defined by Eq. (8), b is the reference size of the structure cross-section, c_D is the drag coefficient evaluated neglecting the transient character of the wind field [13].
Coherently with [26, 27], the integration of the equations of motion is performed in the state space by introducing a Hamming windowing at the beginning of the wind loading history in order to avoid initial transient effects. Each time step Δt = 0.1 s is divided into 10 parts and a linear interpolation of the wind loading is applied. The drag coefficient is evaluated by the Italian Guide on Wind actions and effects on structures [51]. The aerodynamic damping is disregarded.
Differently from [27], where TDA was carried out taking the first two modes of vibration into account, the following evaluations retain the contribution of the sole first mode. This choice aims at establishing the best comparison between TDA and TRST [26], which involves only the contribution of the first mode. It is further supported by [27], where it was shown that the error due to disregarding the second mode is about 1% for structures S1 and S3 whereas it reaches 5-6% for structure S2. Additional estimates of the multi-modal response of structure S2 to synoptic winds showed that this is not due to the transient nature of thunderstorm outflows, but to the fact that this structure is made up of two shafts

and its second mode roughly corresponds to the first mode of the upper shaft (Fig. 1).

Fig. 5 shows the first modal force (a) and the first modal displacement of structure S3 for the simulated thunderstorm outflow in Fig. 4; schemes (b) and (c) refer respectively to $\xi = \xi_a = 0.02$ and $\xi = \xi_b = 0.005$. The growth of the amplitude of the oscillations due to reducing damping confirms that despite the transient features of loading, the structural response exhibits a clear resonant component [27].

This remark is strengthened by means of a systematic analysis of the 3 structure test cases described in Section 2. Accordingly, 93,000 values of the maximum displacement at the top of each structure are evaluated for the 4 wind velocity profiles considered here; 2 damping coefficients are studied. Thus, all in all, 93,000×3×4×2=2,232,000 values of $x_{max}(H)$ are extracted and analysed probabilistically. Tables 3 and 4 summarize the mean values and the coefficients of variation (cov) of $x_{max}(H)$, respectively.

Figs. 6 and 7 show, respectively, the PDF (each bar height is equal to the number of observations in a bin divided by the total number of observations and by the width of the bin) of $x_{max}(H)$ of structure S1 for a wind velocity profile with z_m = 50 m and of structure S3 for z_m = 100 m. Schemes (a) and (b) correspond to $\xi = \xi_a$ and $\xi = \xi_b$, respectively.

Ref. [27] proved that the PDF of $x_{max}(H)$ due to thunderstorm outflows is much more spread than that corresponding to extra-tropical cyclones; such spread tends to increase on decreasing the damping. This remark strengthens a key property of the structural response to downbursts: differently from classic synoptic winds it is not appropriate, or at least it is much more approximated, to identify the maximum value of the response with its mean value [52].

5. EQUIVALENT TIME-DOMAIN ANALYSIS

Embedding EWST (Section 5.1) into hybrid simulation (Section 4.1) produces a drastic simplification referred to as equivalent hybrid simulation (Section 5.2).

5.1. Equivalent Wind Spectrum Technique

The EWST introduced in [28] and refined in [29] with regard to slender structures is a method that drastically reduces the computational burden for evaluating the wind-induced response of structures to stationary winds. It replaces the actual turbulent field, as a random function of time and space, by an equivalent turbulent fluctuation, as a random function of time identically coherent in space. This

quantity is defined in such a way that the first modal loading and aerodynamic admittance associated with the equivalent turbulence match, at their best, those involved by the actual turbulent field.

The generalization of EWST to transient thunderstorm outflows was introduced in [26] assuming that the coherence function of $\tilde{v}'$ is expressed by Eq. (11) whereas no hypothesis is needed on its PSD. Accordingly, the reduced equivalent turbulent fluctuation $\tilde{v}'_{eq}$ is defined by its PSD:

$$S_{\tilde{v}',eq}(n,\delta) = S_{\tilde{v}'}(z_{eq},n)\,C(\delta n) \tag{17}$$

where $S_{\tilde{v}'}$ is the PSD of $\tilde{v}'$, z_{eq} is the so-called equivalent height, C is a frequency filter that takes into account the coherence function of $\tilde{v}'$, in equivalent terms, by reducing its PSD:

$$C(\eta) = \frac{1}{\eta} - \frac{1}{2\eta^2}\left(1 - e^{-2\eta}\right) \quad (\eta > 0) \quad ; \qquad C(0) = 1 \tag{18}$$

η is the argument of C; δ is a time, incorrectly defined a length in [26], referred to as the size factor:

$$\delta = \frac{\kappa c_z H}{\overline{v}_{max}(z_{eq})} \tag{19}$$

κ is a non-dimensional coefficient referred to as the modal shape factor. Dealing with stationary winds and slender vertical cantilever structures, whose first modal shape may be approximated as $\psi_1(z) = (z/H)^{\zeta}$, the equivalent height and the modal shape factor are given by [29]:

$$z_{eq} = 0.6H \quad ; \qquad \kappa = \frac{0.5}{(\zeta+1)^{0.55}} \tag{20}$$

It is worth noting the conceptual meaning of Eq. (19) and its dual time-space interpretation: δ can be regarded as the equivalent time [53, 54] on which the peak wind velocity is averaged to take into

account the equivalent length of the structural part on which the random wind field is coherently applied. Using this formulation Eq. (8) may be rewritten as:

$$v_{eq}(z,t,\delta) = \overline{v}_{max}(h)\alpha(z)\gamma(t)\left[1+\overline{I}_v(h)\beta(z)\mu(t)\tilde{v}'_{eq}(t,\delta)\right] \tag{21}$$

where v_{eq} is the equivalent wind velocity written as an explicit function of δ to point out the key role of this parameter. This expression does not modify the slowly-varying mean part of v whereas it drastically changes its residual fluctuation by replacing the 2-D (Dimensional) process $\tilde{v}'(z,t)$ by the equivalent 1-D process $\tilde{v}'_{eq}(t,\delta)$. The evolution from Eq. (8) to Eq. (21) is a formidable simplification whose correctness was proved in [26] by stressing that, though used in the non-stationary field, EWST is strictly applied to the sole stationary part of turbulent fluctuations.

5.2. Equivalent Hybrid Simulation

The simplification described in Section 5.1 deeply reflects on the hybrid simulation summarised in Table 2. Its evolution, referred to as equivalent hybrid simulation, avoids the factorization of the PSD matrix of $\tilde{v}'$ and involves the simulation of mono-variate sample functions of $\tilde{v}'_{eq}(t,\delta)$ instead of multi-variate sample vectors of $\tilde{v}'(z,t)$. Table 5 shows the main steps of the new simulation algorithm. The advantages in terms of computational burden are huge.

In Ref. [26] no systematic evaluation of the errors involved by EWST was carried out. In addition, since EWST was embedded within other simplifications, it was not possible to enucleate the errors implied by its application. In that framework, especially the use of the equivalent height introduced for an ABL profile also with regard to the nose-shaped one was deemed as a potential source of approximations.

To clarify these implications, also in this case 93,000 values of the maximum displacement at the top of each of the 3 structure test cases are evaluated for each of the 4 wind velocity profiles considered here; 2 damping coefficients are studied. All in all, 93,000×3×4×2=2,232,000 values of $x_{max}(H)$ are extracted and analysed probabilistically. Table 6 shows the δ values related to the examined cases.

Fig. 8 shows three sample functions of the equivalent velocity field corresponding to the actual field in Fig. 4 ($z_m = 50$ m). The shape and the trend of the diagrams in Fig. 4 are preserved whereas the high frequency harmonic content is filtered out to take into account, in equivalent terms, the coherence function and the aerodynamic admittance.

Fig. 9 shows the equivalent first modal force (a) corresponding to Fig. 5 and the related first modal displacement of structure S3 for a thunderstorm outflow simulated by EWST; schemes (b) and (c) refer to $\xi = \xi_a = 0.02$ and $\xi = \xi_b = 0.005$, respectively. The qualitative and quantitative similarity of Figs. 5 and 9 is apparent.

Tables 7 and 8 show, respectively, the mean value and the cov of the $x_{max}(H)$ values provided by the hybrid equivalent simulation. The values in parenthesis are the percent errors committed (with reference to Tables 3 and 4) by EWST. Despite the complexity of the problem dealt with, this error is on average 2-3% and never exceeds 5%. In particular, it is almost surprising the precision with which EWST replicates not only the mean value of $x_{max}(H)$ but also its cov. This aspect was not investigated in previous papers [28, 29], and now strengthens the high reliability of EWST.

Figs. 10-12 enhance the above remarks in the frequency-domain. Fig. 10 shows the modulus of the Fourier transform F_{f1} of the first modal loading of the 3 structure test cases for z_m = 50 m. Figs. 11 and 12 show the modulus of the Fourier transform F_{x1} of the first modal displacement for $\xi = \xi_a$ and $\xi = \xi_b$, respectively. The red lines refer to EWST; the blue lines depict the rigorous solutions. Each diagram is averaged over 93,000 simulations. The different diagrams are almost perfectly overlapped.

Fig. 10 points out that the first modal loading is endowed with two distinct harmonic contents (Eq. 1): the low-frequency one refers to the slowly-varying mean wind velocity $\overline{v}$ whereas the high-frequency one corresponds to the residual turbulent fluctuations v'. The dashed vertical line that ideally separates the two harmonic contents refers to the moving average period $T = 30$ s used to extract $\overline{v}$ from v, i.e. $n = 0.0333$ Hz. Figs. 11 and 12 highlight that the first modal displacement exhibits a clear resonant peak at the frequency n_1 of each structure. Likewise the oscillatory pattern in the schemes (b) and (c) of Figs. 5 and 9, it increases on decreasing the damping. This strengthens a property already noted in [26, 27]: due to the relatively long ramp-up period of thunderstorm outflows, the qualitative behaviour of structures excited by downbursts is not so different from the one that occurs for extra-tropical cyclones.

6. REVISED RESPONSE SPECTRUM TECHNIQUE

Using TRST [26] and assuming that the structural response depends on the sole contribution of the first mode, the maximum value of the displacement x (Eq. (1~~2~~3)) is given by:

$$x_{max}(z) = \hat{x}(z) \cdot S_{d,eq} \tag{22}$$

where $\hat{x}$ is the peak static displacement due to the static action of the peak wind force $\hat{f}$ related to the peak wind velocity $\hat{v}$ (Eq. 9). Based on Eqs. (9), (12)-(16) these quantities are given by:

$$\hat{x}(z) = \frac{1}{m_1 (2\pi n_1)^2} \int_0^H \hat{f}(z) \psi_1(z) dz \tag{23}$$

$$\hat{f}(z) = \frac{1}{2} \rho \hat{v}^2(h) \alpha^2(z) b(z) c_D(z) \tag{24}$$

In addition:

$$S_{d,eq} = d_{eq,max} \tag{25}$$

is the equivalent response spectrum referred to as the maximum value of the modulus of the reduced displacement, d_{eq}, provided by the solution of the differential equation [26]:

$$\ddot{d}_{eq}(t) + 2\xi(2\pi n_1)\dot{d}_{eq}(t) + (2\pi n_1)^2 d_{eq}(t) = (2\pi n_1)^2 u_{eq}^2(t,\delta) \tag{26}$$

where:

$$u_{eq}(t,\delta) = \frac{v_{eq}(h,t,\delta)}{\hat{v}(h)} \tag{27}$$

is the reduced equivalent wind velocity. Ref. [26] provided the procedure, summarized in Appendix A, to evaluate $S_{d,eq}$. It also defined an upper and a lower bound of $S_{d,eq}$: the former is the response spectrum of a point-like SDOF ($\delta = 0$) system; the latter, referred to as the base response spectrum [25], is the response spectrum of a SDOF system subjected to the slowly-varying mean wind velocity $\overline{v}$ ($\delta \to \infty$). All these quantities were identified in [26] by their mean and cov values. While the derivation of this method is rather complex, its application is straightforward: Ref. [26] provided a simple example that showed how to use TRST to calculate the maximum response of a cantilever vertical structure under thunderstorm outflows.

The simulation of an extensive dataset of thunderstorm outflow wind fields coherent with the original measurements, the integration of the equations of motion in the time-domain and the interpretation of a huge amount of results in a probabilistic framework offer a unique opportunity to check the consistency of TRST, to reassess its theoretical and conceptual foundations, and to perform a joint calibration of TRST and TDA. This analysis points out three main issues.

Firstly, the diagrams of the equivalent response spectrum in [26] were affected by an inexactness in the computational procedure that generated them, without any prejudice for the correctness of the method and its background theory. This shortcoming was not detected because the numeric solution was correct for the upper ($\delta = 0$) and lower ($\delta \to \infty$) bounds, where analytical checks were possible. Instead, it caused some inaccuracies for the intermediate values of δ, pointed out by the present cross-check with TDA. Excluding the upper and lower bounds and their surroundings, the correction of this inaccuracy slightly increases $S_{d,eq}$ and accentuates its decrease on increasing n_1 (Fig. 13).

Secondly, two alternative forms of $S_{d,eq}$ were provided in [26]. The first was expressed in terms of n_1 and δ, the second of their reduced values $\tilde{n}_1 = n_1 z_{eq} / \overline{v}_{max}\left(z_{eq}\right)$ and $\tilde{\delta} = \delta \overline{v}_m\left(z_{eq}\right) / z_{eq}$. Based on conceptual arguments the non-dimensional representation was judged more effective than the dimensional one. This statement was strengthened by the analysis of the 93 thunderstorm outflow velocity records [22] that generated the response spectra: from these records it seemed reasonable to express the PSD of $\tilde{v}'$ as a function of the reduced frequency $\tilde{n} = nz / \overline{v}_{max}\left(z\right)$.

Instead, TDA shows now that the first choice is better than the second. This seems to be interpretable in the light of the new findings reported in [55] by examining a richer dataset of 247 thunderstorm outflow

records. They prove that parameterizing the PSD of $\tilde{v}'$ by $\tilde{n} = nz / \overline{v}_{max}(z)$ is not the best choice and better results are found by expressing $S_{\tilde{v}'}$ as a function of $\tilde{n} = nL_v(z) / \overline{v}_{max}(z)$, L_v being the integral length scale of $\tilde{v}'$ determined through its auto-correlation function [56].

This fact does not contradict the discussion in [26] on the opportunity of expressing $S_{d,eq}$ as a function of $\tilde{n}_1$ and $\tilde{\delta}$. However, it raises a new difficult issue: the parameterization of the response as a function of $\tilde{n}_1 = n_1 L_v(z_{eq}) / \overline{v}_{max}(z_{eq})$ replaces the objective parameter z_{eq} by a quantity, $L_v(z_{eq})$, whose evaluation is very uncertain without direct measurements [38, 56]. In other words, it transfers the uncertainties from the calculation of $S_{d,eq}$ to that of $\tilde{n}_1$ [57]. Thus, looking forward to study this issue in major detail, at present it seems more appropriate to express $S_{d,eq}$ as a function of n_1 and δ.

Figs. 13 and 14 show, respectively, the mean value and the cov of $S_{d,eq}$ for 93 thunderstorm outflows recorded in the Ports of Genoa, La Spezia and Livorno in the period 2011-2012 [22]. Schemes (a)-(c) refer, respectively, to ξ = 0.002, 0.01, 0.05. The different diagrams correspond to the parametric variation of δ. The upper diagrams refer to $\delta = 0$, the lower ones to $\delta \to \infty$. As anticipated, the mean value of $S_{d,eq}$ for average δ values decreases on increasing n_1, due to aerodynamic admittance; this trend, not so apparent in [26], is coherent with the response of structures to synoptic winds. As far as concerns scheme (d), it provides the quasi-static equivalent response spectrum defined as:

$$S_{d,qs} = d_{qs,max} \tag{28}$$

This quantity represents the maximum value of the modulus of the quasi-static reduced displacement, namely the quasi-static solution of Eq. (26):

$$d_{qs}(t) = u_{eq}^2(t, \delta) \tag{29}$$

Accordingly, let as introduced the amplification factor defined as:

$$A = \frac{\langle S_{d,eq} \rangle}{\langle S_{d,qs} \rangle} \tag{30}$$

Fig. 15 shows this quantity as extracted from Fig. 13. As for the dynamic response to synoptic winds, *A* tends to decrease on increasing n_1, ξ and δ; in any case $A \geq 1$.

Thirdly, different from synoptic winds for which the PDF of the maximum value of the response is so narrow and sharp that can be confused with its mean value, the remarks in Section 4 confirm [27] that the PDF of the maximum value of the response to thunderstorm outflows is so much spread that its first two statistical moments may be not enough representative. This calls for the opportunity of completing its description by the third and fourth statistical moments or by the PDF itself.

Similarly to Figs. 13 and 14, Figs. 16 and 17 show, respectively, the skewness γ and the kurtosis κ of $S_{d,eq}$. The irregularity of these diagrams depends on the property according to which, on increasing the order of statistical moments, the number of samples from which they are extracted should be increased.

To complete this information, Figs. 18 and 19 show $S_{d,eq}$ diagrams for various exceeding probabilities *P*, respectively, for δ = 1 and 20 s. In addition, they show the mean value of $S_{d,eq}$ plus a number *k* of standard deviations:

$$S_{d,eq} = \langle S_{d,eq} \rangle \left[1 + k \cdot cov\left(S_{d,eq} \right) \right] \qquad (k = 0,1,2) \tag{31}$$

Diagrams with $k = 0,1,2$ roughly correspond to $P = 0.5, 0.8, 0.95$. This information is useful to define a conventional design response spectrum [26] or to develop performance-based analyses [58, 59].

7. RESPONSE SPECTRUM TECHNIQUE VS TIME-DOMAIN ANALYSIS

Tables 9 and 10 summarize the results of the application of TRST illustrated in Section 6. The values in parenthesis are the percent errors committed with respect to TDA (Tables 3 and 4) treated here as a reference target.

Firstly, equivalent TDA (Section 5) showed that errors due to EWST are very small if not evanescent. Thus, the errors shown in Tables 9 and 10 are mainly caused by other simplifications and approximations

in TRST. This removes the fear, exhibited in [26], that the nose shape of the wind profile would have probably required an ad hoc calibration of the equivalent height and of the modal shape factor (Eq. (20)). This problem does not occur or it is marginal.

Secondly, no significant error is due to computing $S_{d,eq}$ for a set of discrete values of n_1, ξ and δ, then interpolating these values for specific parameters. Analyses made by computing $S_{d,eq}$ exactly for design parameters, not reported here, show that these errors are very small and scarcely important.

Taking these premises into account, Tables 9 and 10 point out different levels of errors related to the mean value and the cov of the equivalent response spectrum.

As far as concerns the errors committed by determining the mean value of $x_{max}(H)$ by $\langle S_{d,eq} \rangle$, they are so small that, in their regard, TRST can be judged as highly effective. This remark is strengthened by the tremendous conceptual and computational simplifications involved by TRST in comparison to the sequential application of hybrid simulation, even if in its equivalent form, and TDA. Examining these errors more in detail, for average damping values ($\xi = \xi_a$) they do not exceed 3-4%. For low damping values ($\xi = \xi_b$) errors reach 8-9%. In any case, differently from TDA involving EWST (Table 7), TRST underestimates always the structural response. Errors are almost independent of the wind speed profile.

Regarding the errors committed by determining the cov of $x_{max}(H)$ by $\mathrm{cov}(S_{d,eq})$, they are so large (up to 50%) that cannot be explained other than in relation to conceptual differences between TRST and TDA. An inspection of the conceptual framework of these two methods highlights two reasons potentially capable of justifying such differences: the use of different reference values of the wind speed and of different methods to reconstruct the thunderstorm outflow velocity field starting from individual velocity records. These two issues are discussed in Sections 8 and 9, respectively.

8. EQUIVALENT "MEAN" RESPONSE SPECTRUM

The definition of the reference wind speed is a key issue of TRST since it reflects on the definition of the equivalent response spectrum. This problem, dealt with in [25], led to two alternative approaches.

Following the first, used in [26] and in previous sections, the maximum displacement (Eq. (22)) is the product of the peak static displacement (Eqs. (23) and (24)) by the equivalent response spectrum (Eqs. (25)-(27)); such quantity was called in [25] "peak" response spectrum and plays the role of the dynamic

coefficient for synoptic winds [60]. Its application calls for the collection of a historical series of peak wind speed values, its statistical analysis, and the evaluation of a reference value of $\hat{v}$ with assigned return period.

The second approach, introduced in [25] for a SDOF system, but not extended later to NDOF systems as judged to be less effective than the first one, expresses the maximum displacement as the product of the static displacement induced by the maximum value of the slowly-varying mean wind velocity by a so-called "mean" response spectrum; it plays the role of the gust response factor for synoptic winds [61, 62]. This definition calls for the collection of a historical series of maximum slowly-varying mean wind speed values, its statistical analysis, and the evaluation of a reference value of $\overline{v}_{max}$ with assigned return period.

Confirming the reasons stated in [25] to orient TRST towards the first procedure, firstly its capacity of reducing the spread of results, it is worth noting that the simulation strategy developed in [27] started, as it seemed almost unavoidable, from assigning the profile of the slowly-varying mean wind velocity. So, it is not consistent with the definition of the "peak" response spectrum adopted here, but rather fits the conception of the "mean" response spectrum.

To clarify the effective consistency of TRST and TDA, an assessment of the equivalent "mean" response spectrum, $S_{d,eq}^{-}$, is given below. Coherently with the definition given in [25], the maximum value of the displacement x (Eq. (12)) is expressed as:

$$x_{max}(z) = \overline{x}_{max}(z) \cdot S_{d,eq}^{-} \tag{32}$$

where $\overline{x}_{max}$ is the displacement due to the static action of the wind force $\overline{f}_{max}$ ~~due to~~caused by $\overline{v}_{max}$. Based on Eqs. (5), (12)-(16) these quantities are given by:

$$\overline{x}_{max}(z) = \frac{1}{m_1 (2\pi n_1)^2} \int_0^H \overline{f}_{max}(z) \psi_1(z) \, dz \tag{33}$$

$$\overline{f}_{max}(z) = \frac{1}{2} \rho \overline{v}_{max}^2(h) \alpha^2(z) b(z) c_D(z) \tag{34}$$

In addition, coherently with [25], the equivalent "mean" response spectrum is defined as:

$$S_{d,eq}^{-} = G_v^2(h)\, S_{d,eq} \tag{35}$$

where G_v is the velocity gust factor. Likewise $S_{d,eq}$, also $S_{d,eq}^{-}$ has an upper and a lower bound: the former is the "mean" response spectrum of a point-like ($\delta = 0$) SDOF system; the latter ($\delta \to \infty$) is referred to as the base "mean" response spectrum [25], $S_{d,eq}^{-} = 1$.

Similarly to Figs. 13 and 14, Figs. 20 and 21 show, respectively, the mean value and the cov of $S_{d,eq}^{-}$ for the 93 thunderstorm outflows recorded in the Ports of Genoa, La Spezia and Livorno in the period 2011-2012 [22]. The comparisons of Figs. 20 and 21 with Figs. 13 and 14 show, as expected [21], that $\left\langle S_{d,eq}^{-} \right\rangle > \left\langle S_{d,eq} \right\rangle$ and, averagely, $\mathrm{cov}\left(S_{d,eq}^{-}\right) > \mathrm{cov}\left(S_{d,eq}\right)$.

Tables 11 and 12 show the maximum value of the displacement at the top of the 3 structure test cases provided by Eq. (32) throughout the equivalent "mean" response spectra in Figs 20 and 21. The values in parenthesis are the percent errors committed with reference to the target TDA (Tables 3 and 4).

Confirming the robustness of TRST, the mean values of $x_{max}(H)$ obtained by $\left\langle S_{d,eq}^{-} \right\rangle$ (Table 11) are almost coincident with those obtained by $\left\langle S_{d,eq} \right\rangle$ (Table 9); both represent very good approximations, especially for structures endowed with larger damping, of the mean values provided by the target TDA (Table 3). The use of $\mathrm{cov}(S_{d,eq}^{-})$ greatly increases the spread of the solutions and improves the agreement between the cov of $x_{max}(H)$ in Table 12 and that in Table 10:errors do not exceed 15%.

These evaluations are relevant to clarify that the agreement between TRST and TDA definitely increases by using these methods with similar bases. On the other hand, they do not modify the judgment expressed in [25]: the use of the (peak) response spectrum (Section 6) seems to be better than the "mean" response spectrum just because it reduces the spread of the solution.

9. PROBABILISTIC ASSESSMENT OF THE EQUIVALENT RESPONSE SPECTRUM

The procedure introduced in [26] (Appendix A) to derive the equivalent (peak) response spectrum is a pillar of TRST. It starts from a set of single real wind velocity records of thunderstorm outflows and uses a deterministic tool, the Fourier transform, to re-construct, around each record, first an equivalent

velocity field, then an equivalent (peak) response spectrum. The hybrid simulation introduced in [27] uses instead a probabilistic tool, Monte Carlo simulations, to re-construct, around each record, first a family of 1,000 artificial equivalent velocity fields, then as many scenarios of the maximum response. In order to investigate if the spread of the results obtained through TRST (Tables 10 and 12) is lower than that given by the target TDA (Table 4) due to this difference, Appendix B depicts a probabilistic assessment of the equivalent response spectrum that is almost fully coherent with hybrid simulation.

Based on this probabilistic framework, the mean value and the cov of $S_{d,eq}$ and $S_{d,eq}^{-}$, not reported here, exhibit values qualitatively and quantitatively similar to those obtained by the deterministic method (Figs. 13, 14, 20 and 21). Accordingly, the application of the probabilistic approach to the 3 test case structures in Section 2, not reported here, provides similar results to the ones shown in Tables ~~13~~ 9 to ~~16~~12. More precisely, despite some unavoidable detachments from the deterministic TRST – e.g. the use of a theoretical PSD of $\tilde{v}'$ (Eq. (10)) - the probabilistic approach does not lead to any significant change in the mean values whereas it provides a moderate increase of the cov (differences from Table 4 are now in the order of 10-15%).

These results confirm the robustness of the revised TRST, proving that 93 thunderstorm records represent a reasonable starting point to extract preliminary but representative equivalent response spectra. The agreement between the cov values provided by the probabilistic evaluation of the equivalent "mean" response spectrum and the target TDA proves that starting from common bases these two methods substantially agree despite their conceptual and operative diversities and the complexity of the physical phenomenon examined.

This ~~result~~remark, however, cannot divert attention from two key points. Firstly, a TRST that minimizes the spread of solutions (Section 6) is conceptually superior to a TRST that pursues a better agreement with TDA by increasing such spread (Section 8). Secondly, even if evaluating the equivalent response spectrum in a probabilistic framework (Section 9) improved the agreement with TDA, it would denature the original spirit of the response spectrum technique which is by its own nature deterministic.

10. CONCLUSIONS AND PROSPECTS

This paper examines the dynamic response of structures to thunderstorm outflows through a systematic comparison between the application of TRST [25, 26] and TDA [27]. In this context, it clarifies the

approximations involved by these two methods, points out some properties of TDA not highlighted in the previous paper, leads to a critical refinement of TRST. More precisely:

- hybrid simulation is computationally efficient and produces small errors compared with the target model and with the measurements of thunderstorm outflow velocity fields;
- the integration of the equations of motion points out that despite the transient features of the wind loading, structures exhibit a clear resonant response due to the relatively long ramp-up period of thunderstorm outflows;
- the PDF of the maximum value of the response is so spread that its mean value is not enough representative as in the case of synoptic cyclones;
- EWST provides a formidable simplification without introducing relevant errors not only in the mean value of the maximum response but also in its coefficient of variation;
- the diagrams of the equivalent response spectrum in [26] were affected by an inexactness in the computational procedure that generated them, without any prejudice for the correctness of the method and its background theory;
- in [26], the non-dimensional form of the equivalent response spectrum was judged more effective than the dimensional one. New data [55] and TDA prove that the opposite is true due to the uncertainties in determining the integral length scale of turbulence without direct measurements;
- the comparison between the results provided by TRST and TDA shows an excellent agreement between the mean value of the maximum response whereas TRST provides drastically reduced values in terms of its spread;
- this difference arises because hybrid simulation is based on fixing the profile of the slowly-varying mean wind velocity, whereas TRST starts from fixing the peak wind velocity profile; a revised assessment of TRST coherently with TDA preserves the accuracy of the mean value and makes their spread comparable;
- a probabilistic assessment of TRST improves the agreement between the spread involved by the two methods but not the quality of TRST: it increases the spread of results and denature its deterministic spirit.

The main prospects for future research advances concern several lines:

- hybrid simulation might be re-formulated starting from the peak wind velocity profile instead of the maximum value of the moving average;

- the wind field model should be revised based on better data on the vertical profile of the wind speed and its evolution;
- a criterion should be identified to predict the integral scale of turbulence in order to come back to the initial idea, not implemented in this paper, of expressing the equivalent response spectrum as a function of appropriate dimensionless parameters;
- considering that an extensive catalogue of thunderstorm outflows is now available [55], it is timely to re-evaluate the equivalent response spectrum, studying the influence of the gust front duration;
- all the data used in this paper have been detected in the High Tyrrhenian Sea area; it is fundamental to ascertain if these data can be generalized to different areas by appropriate scaling procedures, or if downbursts in other areas involve different features;
- TRST is calibrated to determine the maximum structural displacement and an equivalent static force consistent with it; it is timely to generalize this procedure to determine refined estimates of other wind loading effects such as bending moments and shear forces.

Taking advantage of the wealth of information gathered, an evolutionary spectral density of thunderstorm outflows coherent with measurements is currently studied to evaluate the transient response of structures through random dynamics. This would give rise to a triad of methods – response spectrum technique, time-domain analysis and evolutionary power spectrum – to be used jointly or alternatively according to the properties of the problem dealt with and with the aims of the solution.

APPENDIX A. Assessment of the equivalent response spectrum

The assessment of the equivalent response spectrum consists of the following 8 steps [26]:

1) Consider the wind velocity $v(h,t)$ recorded during a thunderstorm outflow at the height $z = h$ and decompose it by Eq. (8), with $\alpha(h)=\beta(h)=1$; extract the reduced turbulent fluctuation $\tilde{v}'(h,t)$ and the peak wind velocity $\hat{v}(h)$.
2) Evaluate the Fourier Transform of $\tilde{v}'(h,t)$, namely $\tilde{V}'(h,n)=F\{\tilde{v}'(h,t)\}$.
3) Evaluate the Fourier Transform of the reduced equivalent turbulent fluctuation $\tilde{v}'_{eq}(t,\delta)$ by:

$$\tilde{V}'_{eq}(n,\delta)=\tilde{V}'(h,n)\sqrt{C(\delta n)} \tag{A.1}$$

C being the filter operator and δ the size factor defined by Eqs. (18) and (19), respectively.

4) Evaluate $\tilde{v}'_{eq}(t,\delta)$ as the inverse Fourier transform of $\tilde{V}'_{eq}(n,\delta)$, namely $\tilde{v}'_{eq}(t,\delta)=F^{-1}\left\{\tilde{V}'_{eq}(n,\delta)\right\}$.

5) Replace $\tilde{v}'_{eq}(t,\delta)$ into Eq. (21), with $\alpha(h)=\beta(h)=1$, and evaluate the equivalent velocity $v_{eq}(h,t,\delta)$.

6) Replace $v_{eq}(h,t,\delta)$ and $\hat{v}(h)$ into Eq. (27) and evaluate the reduced equivalent velocity $u_{eq}(t,\delta)$.

7) Replace $u_{eq}(t,\delta)$ into Eq. (26) and evaluate the reduced displacement $d_{eq}(t)$.

8) Solve Eq. (26) and evaluate the equivalent response spectrum $S_{d,eq}$ (Eq. (25)).

Repeat these evaluations for a suitable grid of realistic parameters δ, n_1, ξ.

APPENDIX B. Probabilistic assessment of the equivalent response spectrum

The probabilistic assessment of the equivalent (peak) response spectrum consists of the following 8 steps:

1) Consider the wind velocity $v(h,t)$ recorded during a thunderstorm outflow at the height $z = h$ and decompose it by Eq. (8), with $\alpha(h)=\beta(h)=1$; extract the reduced turbulent fluctuation $\tilde{v}'(h,t)$ and the peak wind velocity $\hat{v}(h)$.

2) Assign the PSD of $\tilde{v}'(h,t)$, $S_{\tilde{v}'}(h,n)$, by Eq. (10).

3) Use Eq. (17) to evaluate the PSD of the reduced equivalent turbulent fluctuation $\tilde{v}'_{eq}(t,\delta)$, $S_{\tilde{v}',eq}(n,\delta)$, C being the filter operator and δ the size factor defined by Eqs. (18) and (19), respectively.

4) Perform a Monte Carlo simulation aiming to generate L artificial time-histories $\tilde{v}'_{eq}(t,\delta)$.

5) Replace the L time-histories $\tilde{v}'_{eq}(t,\delta)$ into Eq. (21), with $\alpha(h)=\beta(h)=1$, and generate L equivalent wind velocities $v_{eq}(h,t,\delta)$.

6) Replace $v_{eq}(h,t,\delta)$ and $\hat{v}(h)$ into Eq. (27) and evaluate L reduced equivalent velocities $u_{eq}(t,\delta)$.

7) Replace each $u_{eq}(t,\delta)$ into Eq. (26) and determine L reduced displacements $d_{eq}(t)$.

8) Solve Eq. (26) and evaluate L equivalent response spectra $S_{d,eq}$ (Eq. (25)).

Repeat these evaluations for a suitable grid of realistic parameters δ, n_1, ξ.

The probabilistic assessment of the equivalent "mean" response spectrum implies one more step:

9) Apply Eq. (35) and determine the equivalent "mean" response spectrum $S^{-}_{d,eq}$.

APPENDIX C. List of main symbols and acronyms

List of symbols:

A	amplification factor defined by Eq. (30);
b	width of the structural surface exposed to wind;
c_D	drag coefficient;
c_z	exponential decay coefficient of $\tilde{v}'$ along z;
$Coh_{\tilde{v}'\tilde{v}'}$	coherence function of $\tilde{v}'$ (Eqs. ~~7 and~~ 11);
d	reduced displacement;
f, f_k	force and k-th modal force (Eqs. 16 and 15);
G_v	velocity gust factor (Eq. 9);
h, H	reference height of the wind velocity and height of the structure;
I_v, L_v	reduced turbulence intensity and integral length scale;
m, m_k	mass per unit length and k-th modal mass (Eq. 14);
n, n_k, n_c	frequency, k-th frequency and cut-off frequency;
p_k	k-th principal coordinate;
$S_{\tilde{v}'\tilde{v}'}, S_{\tilde{v}'}$	CPSD (Eq. 7) and PSD (Eq. 10) of $\tilde{v}'$;
S_d, S_d^-	(peak) and "mean" response spectra;
t, T	time and moving average period;
u, v	reduced wind velocity and wind velocity;
$\tilde{V}'$	Fourier transform of $\tilde{v}'$;
x	structural displacement;
$z, z'; z_m$	heights above ground; height at which the wind velocity is maximum;
α, β	non-dimensional functions that define the shape of $\bar{v}(z)$ (Eq. 5) and $I_v(z)$ (Eq. 6);
δ, κ	size factor (Eq. 19) and modal shape factor (Eq. 20);
γ, μ	non-dimensional functions that define the time variation of $\bar{v}$ (Eq. 5) and I_v (Eq. 6);
ρ	density of air;
σ_v	slowly-varying standard deviation of the residual velocity fluctuation v' (Eq. 2);

τ short time interval over which the peak wind velocity $\hat{v}$ is averaged;

ξ damping coefficient;

ψ_k k-th mode of vibration;

ζ exponent of the power law that approximates ψ_1;

$\Delta n, \Delta t$ time and frequency step;

ΔT time interval between 10 minutes and 1 hour.

Indexes, Apexes and Operators:

$\bullet_{max}, \bullet_{eq}, \bullet_{qs}$ maximum, equivalent and quasi-static;

$\bullet', \hat{\bullet}, \tilde{\bullet}, \overline{\bullet}$ fluctuating, peak (over τ), reduced (non-dimensional) and (temporal) mean;

$\langle \bullet \rangle, \mathrm{cov}(\bullet)$ ensemble mean and coefficient of variation;

$C(\bullet)$ operator defined by Eq. (18);

$F\{\bullet\}, F^{-1}\{\bullet\}$ Fourier and inverse Fourier transforms.

List of Acronyms:

ABL	Atmospheric Boundary Layer;
EWST	Equivalent Wind Spectrum Technique;
PDF	Probability Density Function;
POD	Proper Orthogonal Decomposition;
PSD, CPSD, EPSD	Power Spectral Density, Cross-PSD and Evolutionary PSD;
SDOF, NDOF	Single- and N-Degree-Of-Freedom;
TDA	Time-Domain Analysis;
TRST	Thunderstorm Response Spectrum Technique.

ACKNOWLEDGEMENTS

This research is funded by the European Research Council (ERC) under the European Union's Horizon 2020 research and innovation program (grant agreement No. 741273) for the project THUNDERR - Detection, simulation, modelling and loading of thunderstorm outflows to design wind-safer and cost-efficient structures – supported by an Advanced Grant 2016. The data exploited have been recorded by the monitoring network realized for the European Projects "Winds and Ports" (grant No. B87E09000000007)

and “Wind, Ports and Sea” (grant No. B82F13000100005), funded by the European Territorial Cooperation Objective, Cross-border program Italy-France Maritime 2007-2013.

REFERENCES

[1] Letchford CW, Mans C, Chay MT. Thunderstorms – their importance in wind engineering (a case for the next generation wind tunnel). J Wind Eng Ind Aerod 2002; 90: 1415-1433.

[2] Solari G. Emerging issues and new scenarios for wind loading on structures in mixed climates. Wind Struct 2014; 19: 295-320.

[3] Davenport AG. The application of statistical concepts to the wind loading of structures. Proc Inst Civ Eng 1961; 19: 449-472.

[4] Byers HR, Braham RR. The thunderstorm: Final report of the Thunderstorm Project. U.S. Government Printing Office, Washington, DC, 1949.

[5] Goff RG. Vertical structure of thunderstorm outflows. Mon Wea Rev 1976; 104: 1429-1440.

[6] Hjelmfelt MR. Structure and life cycle of microburst outflows observed in Colorado. J Appl Meteorol 1988; 27: 900-927.

[7] Fujita TT. Downburst: meteorological features and wind field characteristics. J Wind Eng Ind Aerod 1990; 36: 75-86.

[8] Choi ECC, Hidayat FA. Dynamic response of structures to thunderstorm winds. Prog Struct Eng Mat 2002; 4: 408-416.

[9] Chen L, Letchford CW. Parametric study on the alongwind response of the CAARC building to downbursts in the time domain. J Wind Eng Ind Aerod 2004; 92: 703-724.

[10] Holmes J, Forristall G, McConochie J. Dynamic response of structures to thunderstorm winds. Proc 10th Americas Conference on Wind Engineering, Baton Rouge, Louisiana, USA, 2005.

[11] Chay MT, Albermani F, Wilson B. Numerical and analytical simulation of downburst wind loads. Eng Struct 2006; 28: 240-254.

[12] Chen X. Analysis of alongwind tall building response to transient nonstationary winds. J Struct Eng ASCE 2008; 134: 782-791.

[13] Kwon DK, Kareem A. Gust-front factor: new framework for wind load effects on structures. J Struct Eng ASCE 2009; 135: 717-732.

[14] Le TH, Caracoglia L. Reduced-order wavelet-Galerkin solution for the coupled, nonlinear stochastic response of slender buildings in transient winds. J Sound Vibr 2015; 344: 179-208.

[15] Le TH, Caracoglia L. Computer-based model for the transient dynamics of a tall building during digitally simulated Andrews AFB thunderstorm. Comp Struct 2018; 193: 44-72.

[16] Wang L, McCullough M, Kareem A. A data-driven approach for simulation of full-scale downburst wind speeds. J Wind Eng Ind Aerod 2013; 123: 171-190.

[17] Huang G, Zheng H, Xu YL, Li Y. Spectrum models for non-stationary extreme winds. J Struct Eng ASCE 2015; 141: 04015010.

[18] Peng L, Huang G, Chen X, Kareem A. Simulation of multivariate nonstationary random processes: hybrid stochastic wave and proper orthogonal decomposition approach. J Eng Mech ASCE 2017; 143: 04017064.

[19] Solari G, Repetto MP, Burlando M, De Gaetano P, Pizzo M, Tizzi M, Parodi M. The wind forecast for safety and management of port areas. J Wind Eng Ind Aerod 2012; 104-106: 266-277.

[20] Repetto MP, Burlando M, Solari G, De Gaetano P, Pizzo M, Tizzi M. A GIS-based platform for the risk assessment of structures and infrastructures exposed to wind. Adv Eng Softw 2018; 117: 29-45.

[21] De Gaetano P, Repetto MP, Repetto T, Solari G. Separation and classification of extreme wind events from anemometric records. J Wind Eng Ind Aerod 2014; 126: 132-143.

[22] Solari G, Burlando M, De Gaetano P, Repetto MP. Characteristics of thunderstorms relevant to the wind loading of structures. Wind Struct 2015; 20: 763-791.

[23] Housner GW. Behavior of structures during earthquakes. J Mech Div ASCE 1959; 85: 109-129.

[24] Solari G. Wind response spectrum. J Eng Mech ASCE 1989; 115: 2057-2073.

[25] Solari G, De Gaetano P, Repetto MP. Thunderstorm response spectrum: fundamentals and case study. J Wind Eng Ind Aerod 2015; 143: 62-77.

[26] Solari G. Thunderstorm response spectrum technique: theory and applications. Eng Struct 2016; 108: 28-46.

[27] Solari G, Rainisio D, De Gaetano P. Hybrid simulation of thunderstorm outflows and wind-excited response of structures. Meccanica 2017; 52: 3197–3220.

[28] Solari G. Equivalent wind spectrum technique: theory and applications. J Struct Eng ASCE 1988; 114: 1303-1323.

[29] Piccardo G, Solari G. Generalized equivalent spectrum technique. Wind Struct 1998; 1: 161-174.

[30] Chen L, Letchford CW, A deterministic-stochastic hybrid model of downbursts and its impact on a cantilevered structure. Eng Struct 2004; 26: 619-629.

[31] Holmes JD, Hangan HM, Schroeder JL, Letchford CW, Orwig KD. A forensic study of the Lubbock-Reese downdraft of 2002. Wind Struct 2008; 11: 19-39.

[32] Oseguera RM, Bowles RL. A simple analytic 3-dimensional downburst model based on boundary layer stagnation flow. NASA Technical Memorandum 100632, 1988.

[33] Vicroy DD. Assessment of micro burst models for downdraft estimation. J Aircraft 1992; 29: 1043-1048.

[34] Wood GS, Kwok KCS. An empirically derived estimate for the mean velocity profile of a thunderstorm downburst. Proc 7th Australian Wind Engineering Society Workshop, Auckland, Australia, 1998.

[35] Li C, Li QS, Xiao YQ, Ou JP. A revised empirical model and CFD simulations for 3D axisymmetric steady-state flows of downbursts and impinging jets. J Wind Eng Ind Aerod 2012; 102: 48-60.

[36] Abd-Elaal E, Mills JE, Ma X. An analytical model for simulating steady state flows of downburst. J Wind Eng Ind Aerod 2013; 115: 53-64.

[37] Holmes JD, Oliver SE. An empirical model of a downburst. Eng Struct 2000; 22: 1167-1172.

[38] Solari G, Piccardo G. Probabilistic 3-D turbulence modeling for gust buffeting of structures. Prob Eng Mech 2001; 16: 73-86.

[39] Li Y, Kareem A. Simulation of multivariate nonstationary random processes by FFT. J Eng Mech ASCE 1991; 117: 1037-1058.

[40] Deodatis G. Non-stationary stochastic vector processes: seismic ground motion applications. Prob Eng Mech 1996; 11: 149-168.

[41] Sakamoto S, Ghanem R. Simulation of multi-dimensional non-Gaussian non-stationary random fields. Prob Eng Mech 2002; 17: 167-176.

[42] Wen YK, Gu P. Description and simulation of nonstationary processes based on Hilbert spectra. J Eng Mech ASCE 2004; 130: 942-951.

[43] Cacciola P, Deodatis G. A method for generating fully non-stationary and spectrum-compatible ground motion vector processes. Soil Dyn Earthq Eng 2011; 31: 351-360.

[44] Huang G. An efficient simulation approach for multivariate nonstationary process: Hybrid of wavelet and spectral representation method. Prob Eng Mech 2014; 37: 74-83.

[45] Carassale L, Solari G. Monte Carlo simulation of wind velocity fields on complex structures. J Wind Eng Ind Aerod 2006; 94: 323-339.

[46] Shinozuka M, Jan CM. Digital simulation of random processes and its applications. J Sound Vibr 1972; 25: 111-128.

[47] Li Y, Kareem A. Stochastic decomposition and application to probabilistic mechanics. J Eng Mech ASCE 1995; 121: 162-174.

[48] Yang JN. On the normality and accuracy of simulated random processes. J Sound Vibr 1973; 26: 417-428.

[49] Di Paola M. Digital simulation of wind field velocity. J Wind Eng Ind Aerod 1998; 74-76: 91-109.

[50] Carassale L, Solari G, Tubino F. Proper Orthogonal Decomposition in wind engineering. Part 2: Theoretical aspects and some applications. Wind Struct 2007; 10: 177-208.

[51] CNR-DT 207/2008. Instructions for assessing wind actions and effects on structures. National Research Council, Rome, Italy, 2009.

[52] Davenport AG. Note on the distribution of the largest value of a random function with application to gust loading. Proc Inst Civ Eng London UK 1964; 24: 187-196.

[53] Greenway ME. An analytical approach to wind velocity gust factors. J Ind Aerod 1979; 5: 61-91.

[54] Solari G. Gust buffeting. I: peak wind velocity and equivalent pressure. J Struct Eng ASCE 1993; 119: 365-382.

[55] Zhang S, Solari G, De Gaetano P, Burlando M, Repetto MP. A refined analysis of thunderstorm outflow characteristics relevant to the wind loading of structures. Prob Eng Mech 2018; 54: 9-24.

[56] Flay RGJ, Stevenson DC. Integral length scales in strong winds below 20 m. J Wind Eng Ind Aerod 1988; 28: 21-30.

[57] Solari G. Wind-excited response of structures with uncertain parameters. Prob Eng Mech 1997; 12: 75-87.

[58] Ciampoli M, Petrini F, Augusti G. Performance-based wind engineering: towards a general procedure. Struct Saf 2011; 33: 367–378.

[59] Spence SMJ, Kareem A. Performance-based design and optimization of uncertain wind-excited dynamic building systems. Eng Struct 2014; 78: 133-144.

[60] Eurocode 1. Actions on structures - General actions. Part 1-4: Wind actions, CEN, EN 1991-1-4, 2015.

[61] Architectural Institute of Japan. AIJ Recommendations for loads on buildings, AIJ, 2004.

[62] International Standards Organization. Wind actions on structures, ISO 4354:2009, 2009.

Table 1. Main properties of the three structure test cases.

Structure	Description	H (m)	n_1 (Hz)	n_2 (Hz)	n_3 (Hz)	ξ_a	ξ_b	N
S1	Steel lighting pole	15.76	0.532	3.186	8.744	0.01	0.002	16
S2	Steel telecommunication antenna mast	36.00	0.821	3.106	5.972	0.01	0.002	19
S3	R.C. telecommunication tower	98.00	0.494	3.167	6.274	0.02	0.005	26

Table 2. Steps of the hybrid simulation technique.

Step	Description
1	Assign h and $\overline{v}_{max}(h)$ by fixing its return period.
2	Select J pairs of $\alpha(z)$ and $\beta(z)$ profiles by a parametric assignment.
3	Extract K pairs of $\gamma(t)$ and $I_v(h,t) = \overline{I}_v(h)\mu(t)$ sample functions from measured records.
4	Use a Monte Carlo algorithm to simulate L sample fields $\tilde{v}'(z,t)$ coherent with the CPSD in Eq. (7).
5	Assemble results by Eq. (8) and obtain $M = J \times K \times L$ sample fields $v(z,t)$.

Table 3. Mean value of the maximum displacement x_{max} (m) at the structure top H by time-domain analysis.

Structure	$\xi = \xi_a$				$\xi = \xi_b$			
	z_m = 25m	z_m = 50m	z_m = 75m	z_m = 100m	z_m = 25m	z_m = 50m	z_m = 75m	z_m = 100m
S1	0.651	0.651	0.643	0.639	0.851	0.853	0.842	0.831
S2	0.326	0.357	0.364	0.370	0.414	0.454	0.465	0.472
S3	0.046	0.072	0.082	0.087	0.055	0.087	0.100	0.106

Table 4. Cov of the maximum displacement x_{max} at the structure top H by time-domain analysis.

Structure	$\xi = \xi_a$				$\xi = \xi_b$			
	z_m = 25m	z_m = 50m	z_m = 75m	z_m = 100m	z_m = 25m	z_m = 50m	z_m = 75m	z_m = 100m
S1	0.242	0.246	0.241	0.240	0.291	0.296	0.290	0.289
S2	0.216	0.218	0.218	0.218	0.259	0.262	0.259	0.263
S3	0.184	0.192	0.195	0.193	0.215	0.227	0.235	0.231

Table 5. Steps of the equivalent hybrid simulation technique.

Step	Description
1	Assign h and $\overline{v}_{max}(h)$ by fixing its return period.
2	Select J pairs of $\alpha(z)$ and $\beta(z)$ profiles by a parametric assignment.
3	Extract K pairs of $\gamma(t)$ and $I_v(h,t) = \overline{I}_v(h)\mu(t)$ sample functions from measured records.
4	Evaluate the size factor δ by Eqs. (19) and (20).
5	Use a Monte Carlo algorithm to simulate L sample functions $\tilde{v}'(t,\delta)$ coherent with the PSD in Eq. (10).
6	Assemble the results by Eq. (21) and obtain $M = J \times K \times L$ sample fields $v_{eq}(z,t,\delta)$.

Table 6. Size factor δ (s).

Structure	z_m = 25m	z_m = 50m	z_m = 75m	z_m = 100m
S1	1.486	1.484	1.483	1.483
S2	2.533	2.469	2.449	2.439
S3	8.273	7.075	6.752	6.602

Table 7. Mean value of the maximum displacement x_{max} (m) at the structure top H by equivalent time-domain analysis (in parenthesis the percent error with reference to Table 3).

Structure	$\xi = \xi_a$				$\xi = \xi_b$			
	z_m = 25m	z_m = 50m	z_m = 75m	z_m = 100m	z_m = 25m	z_m = 50m	z_m = 75m	z_m = 100m
S1	0.670 (+3)	0.665 (+2)	0.658 (+2)	0.654 (+2)	0.880 (+3)	0.874 (+3)	0.862 (+2)	0.856 (+3)
S2	0.335 (+3)	0.362 (+1)	0.374 (+3)	0.377 (+2)	0.427 (+3)	0.462 (+2)	0.476 (+2)	0.482 (+2)
S3	0.046 (-1)	0.070 (-3)	0.079 (-4)	0.084 (-4)	0.054 (-2)	0.083 (-4)	0.095 (-5)	0.101 (-5)

Table 8. Cov of the maximum displacement x_{max} at the structure top H by equivalent time-domain analysis (in parenthesis the percent error with reference to Table 4).

Structure	$\xi = \xi_a$				$\xi = \xi_b$			
	z_m = 25m	z_m = 50m	z_m = 75m	z_m = 100m	z_m = 25m	z_m = 50m	z_m = 75m	z_m = 100m
S1	0.247 (+2)	0.249 (+1)	0.244 (+1)	0.243 (+1)	0.296 (+2)	0.302 (+2)	0.293 (+1)	0.291 (+1)
S2	0.221 (+2)	0.219 (+1)	0.223 (+2)	0.220 (+1)	0.263 (+2)	0.261 (=)	0.262 (+1)	0.263 (=)
S3	0.180 (-2)	0.185 (-4)	0.188 (-4)	0.186 (-4)	0.212 (-2)	0.222 (-2)	0.225 (-4)	0.225 (-3)

Table 9. Mean value of the maximum displacement x_{max} (m) at the structure top H by the revised TRST (in parenthesis the percent error with reference to Table 3).

Structure	$\xi = \xi_a$				$\xi = \xi_b$			
	z_m = 25m	z_m = 50m	z_m = 75m	z_m = 100m	z_m = 25m	z_m = 50m	z_m = 75m	z_m = 100m
S1	0.630 (-3)	0.624 (-4)	0.622 (-3)	0.620 (-3)	0.783(-8)	0.775 (-9)	0.773 (-8)	0.771 (-7)
S2	0.323 (-1)	0.351 (-2)	0.359 (-1)	0.363 (-2)	0.395 (-5)	0.429 (-6)	0.439 (-6)	0.444 (-6)
S3	0.046 (=)	0.071 (-1)	0.080 (-2)	0.085 (-2)	0.053 (-4)	0.081 (-7)	0.092 (-8)	0.097 (-8)

Table 10. Cov of the maximum displacement x_{max} at the structure top H by the revised TRST (in parenthesis the percent error with reference to Table 4).

Structure	$\xi = \xi_a$				$\xi = \xi_b$			
	z_m = 25m	z_m = 50m	z_m = 75m	z_m = 100m	z_m = 25m	z_m = 50m	z_m = 75m	z_m = 100m
S1	0.169(-30)	0.169(-31)	0.169(-30)	0.169(-30)	0.240(-18)	0.240(-19)	0.240(-17)	0.240(-17)
S2	0.142(-34)	0.143(-34)	0.143(-34)	0.143(-34)	0.199(-23)	0.200(-24)	0.200(-23)	0.200(-24)
S3	0.095(-48)	0.099(-48)	0.100(-49)	0.100(-48)	0.142(-34)	0.149(-34)	0.151(-36)	0.152(-34)

Table 11. Mean value of the maximum displacement x_{max} (m) at the structure top H by the equivalent "mean" response spectrum (in parenthesis the percent error with reference to Table 3).

Structure	$\xi = \xi_a$				$\xi = \xi_b$			
	z_m = 25m	z_m = 50m	z_m = 75m	z_m = 100m	z_m = 25m	z_m = 50m	z_m = 75m	z_m = 100m
S1	0.633 (-3)	0.626 (-4)	0.624 (-3)	0.623 (-3)	0.783(-8)	0.775 (-9)	0.773 (-8)	0.771 (-7)
S2	0.325 (=)	0.352 (-1)	0.361 (-1)	0.365 (-1)	0.395 (-5)	0.428 (-6)	0.439 (-6)	0.444 (-6)
S3	0.046 (=)	0.071 (-1)	0.080 (-2)	0.085 (-2)	0.053 (-4)	0.081 (-7)	0.092 (-8)	0.098 (-8)

Table 12. Cov of the maximum displacement x_{max} at the structure top H by the equivalent "mean" response spectrum (in parenthesis the percent error with reference to Table 4).

Structure	$\xi = \xi_a$				$\xi = \xi_b$			
	z_m = 25m	z_m = 50m	z_m = 75m	z_m = 100m	z_m = 25m	z_m = 50m	z_m = 75m	z_m = 100m
S1	0.220(-9)	0.220(-11)	0.220(-9)	0.220(-8)	0.264(-9)	0.264(-11)	0.264(-9)	0.264(-9)
S2	0.203(-6)	0.204(-6)	0.204(-6)	0.204(-6)	0.224(-13)	0.225(-14)	0.225(-13)	0.225(-14)
S3	0.173(-6)	0.177(-8)	0.178(-9)	0.179(-7)	0.191(-11)	0.197(-13)	0.199(-15)	0.200(-13)

FIGURE CAPTIONS

Fig. 1. Wind velocity records v detected in the Port of La Spezia: (a) synoptic extra-tropical cyclone recorded on 7 October 2011; (b) thunderstorm outflow recorded on 25 October 2011.

Fig. 2: Thunderstorm downburst and nose velocity profile in the radial outflow [6].

Fig. 3. Structure test cases [27]: a) steel lighting pole (S1); b) steel telecommunication antenna mast (S2); c) reinforced concrete telecommunication tower (S3).

Fig. 4. Sample functions of a wind velocity field v (z_m = 50 m) at: a) z = 18 m; b) z = 54 m; c) z = 80 m.

Fig. 5. First modal force f_1 (a) and first modal displacements x_1 of structure S3 for the simulated thunderstorm outflow in Fig. 4, being $\xi = \xi_a = 0.02$ (b) and $\xi = \xi_b = 0.005$ (c).

Fig. 6. PDF of the maximum value of the top displacement x_{max} of structure S1 for z_m = 25 m: (a) $\xi = 0.01$ (b) $\xi = 0.002$.

Fig. 7. PDF of the maximum value of the top displacement x_{max} of structure S3 for z_m = 100 m: (a) $\xi = 0.02$; (b) $\xi = 0.005$.

Fig. 8. Sample functions of the equivalent velocity field v_{eq} corresponding to that in Fig. 4 (z_m = 50 m): (a) z = 18 m; (b) z = 54 m; (c) z = 80 m.

Fig. 9. Equivalent first modal force f_1 (a) (corresponding to Fig. 5) and first modal displacements x_1 of structure S3 for a thunderstorm outflow simulated by EWST (Fig. 8) for $\xi = \xi_a = 0.02$ (b) and $\xi = \xi_b = 0.005$ (c).

Fig. 10. Square modulus of the Fourier transform F of the first modal wind loading f_1 (multiplied by the frequency n) averaged over 93,000 simulations (z_m = 50 m): (a) structure S1; (b) structure S2; (c) structure S3 (red lines refer to EWST, blue lines to rigorous solution).

Fig. 11. Square modulus of the Fourier transform F of the first modal displacement x_1 (multiplied by the frequency n) for $\xi = \xi_a$ averaged over 93,000 simulations (z_m = 50 m): (a) structure S1; (b) structure S2; (c) structure S3 (red lines refer to EWST, blue lines to rigorous solution).

Fig. 12. Square modulus of the Fourier transform F of the first modal displacement x_1 (multiplied by the frequency n) for $\xi = \xi_b$ averaged over 93,000 simulations (z_m = 50 m): (a) structure S1; (b) structure S2; (c) structure S3 (red lines refer to EWST, blue lines to rigorous solution).

Fig. 13: Mean value of the equivalent response spectrum: (a) $\xi = 0.002$; (b) $\xi = 0.01$; (c) $\xi = 0.05$; (d) quasi-static solution.

Fig. 14: Cov of the equivalent response spectrum: (a) $\xi = 0.002$; (b) $\xi = 0.01$; (c) $\xi = 0.05$; (d) quasi-static solution.

Fig. 15: Amplification factor: (a) $\xi = 0.002$; (b) $\xi = 0.01$; (c) $\xi = 0.05$.

Fig. 16: Skewness of the equivalent response spectrum: (a) $\xi = 0.002$; (b) $\xi = 0.01$; (c) $\xi = 0.05$; (d) quasi-static solution.

Fig. 17: Kurtosis of the equivalent response spectrum: (a) $\xi = 0.002$; (b) $\xi = 0.01$; (c) $\xi = 0.05$; (d) quasi-static solution.

Fig. 18: Equivalent response spectrum for δ = 1 s, with exceeding probability P: (a) $\xi = 0.002$; (b) $\xi = 0.01$; (c) $\xi = 0.05$

Fig. 19: Equivalent response spectrum for δ = 20 s, with exceeding probability P: (a) $\xi = 0.002$; (b) $\xi = 0.01$; (c) $\xi = 0.05$.

Fig. 20: Mean value of the equivalent "mean" response spectrum: (a) $\xi = 0.002$; (b) $\xi = 0.01$; (c) $\xi = 0.05$.

Fig. 21: Cov of the equivalent "mean" response spectrum: (a) $\xi = 0.002$; (b) $\xi = 0.01$; (c) $\xi = 0.05$.

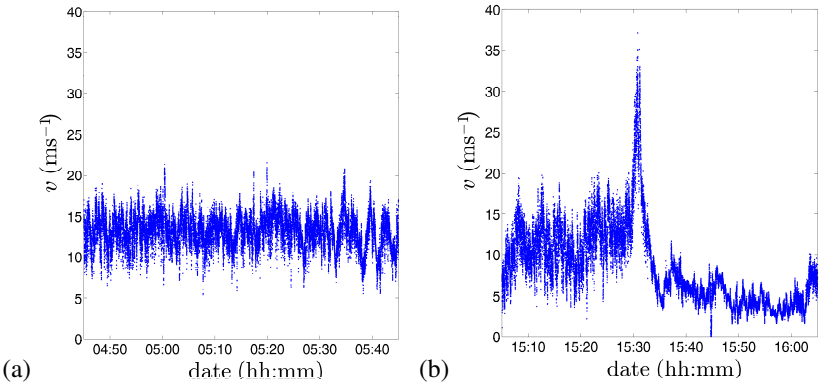

(a) (b)

Fig. 1.

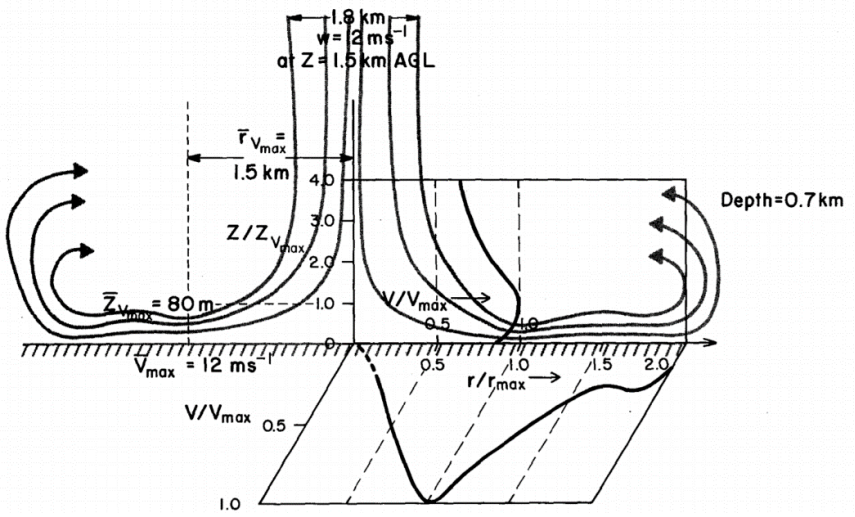

Fig. 2.

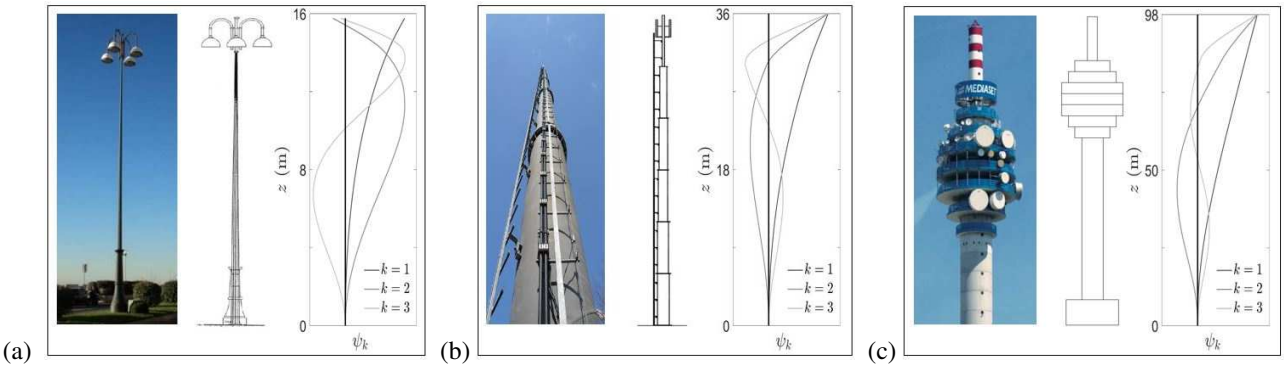

(a) (b) (c)

Fig. 3.

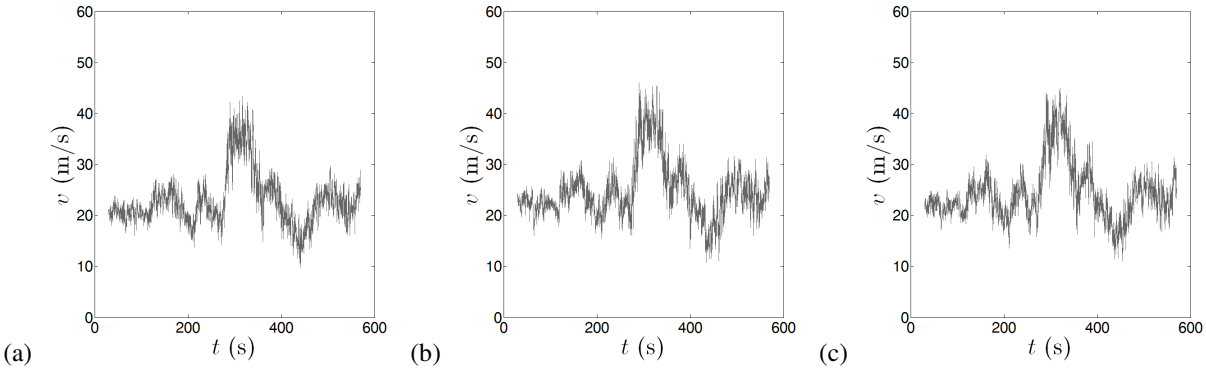
(a)
(b)
(c)
v (m/s)
t (s)
0
10
20
30
40
50
60
200
400
600

Fig. 4.

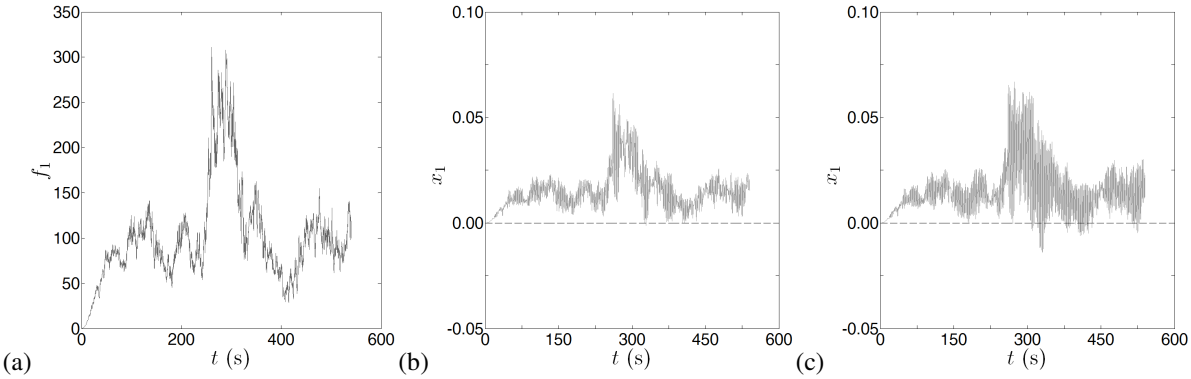
(a)
(b)
(c)
f_1
x_1
t (s)
0
50
100
150
200
250
300
350
0.10
0.05
0.00
-0.05
150
300
450
600

Fig. 5.

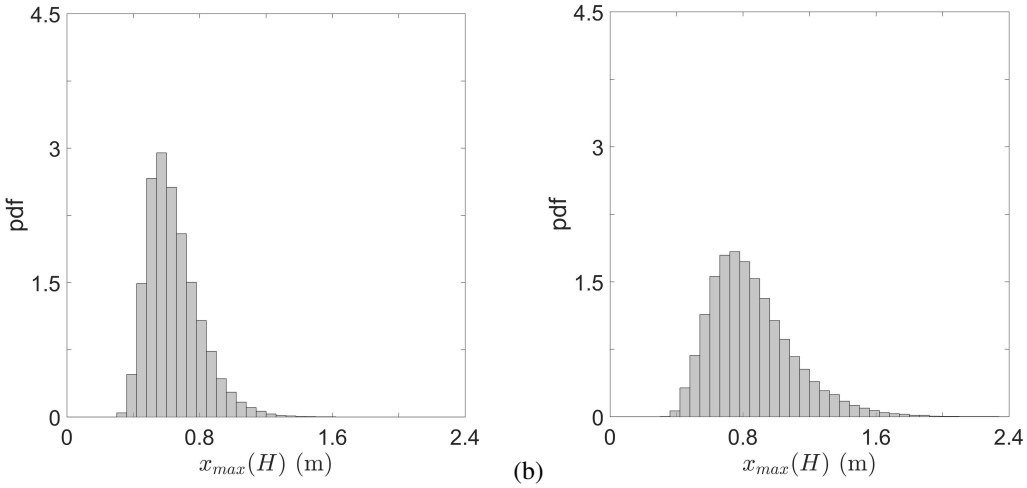

(a) (b)

Fig. 6.

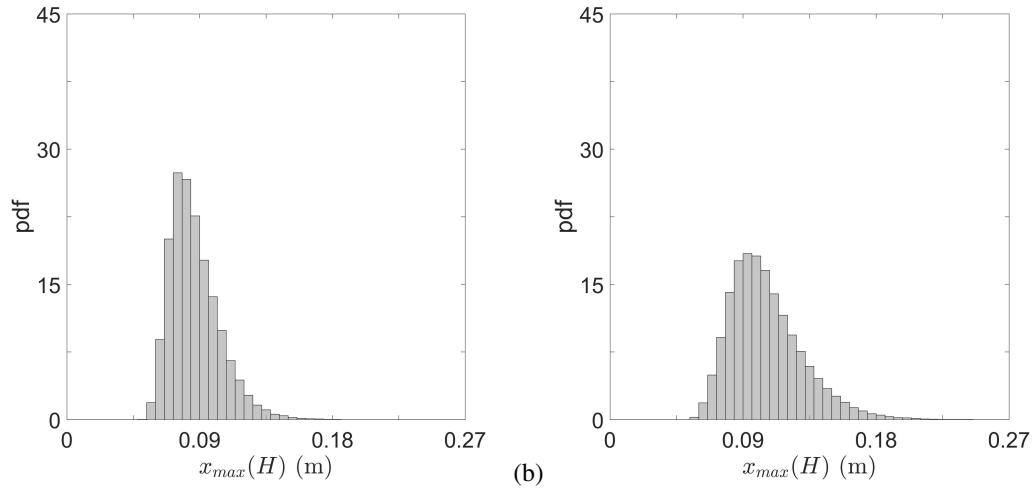

(a) (b)

Fig. 7.

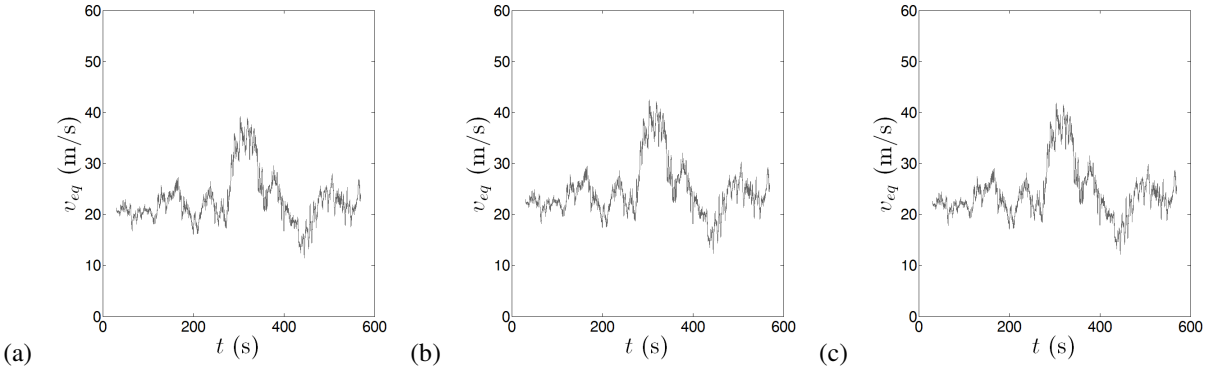

Fig. 8.

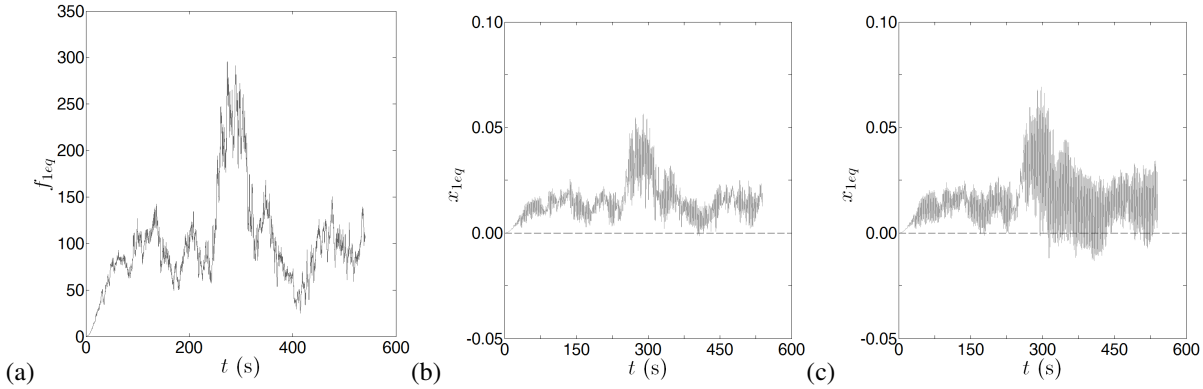

Fig. 9.

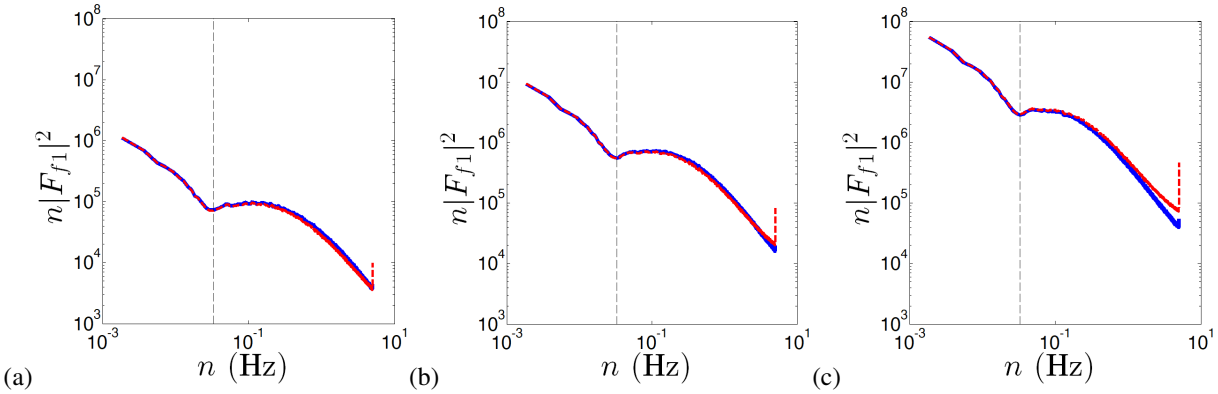

Fig. 10.

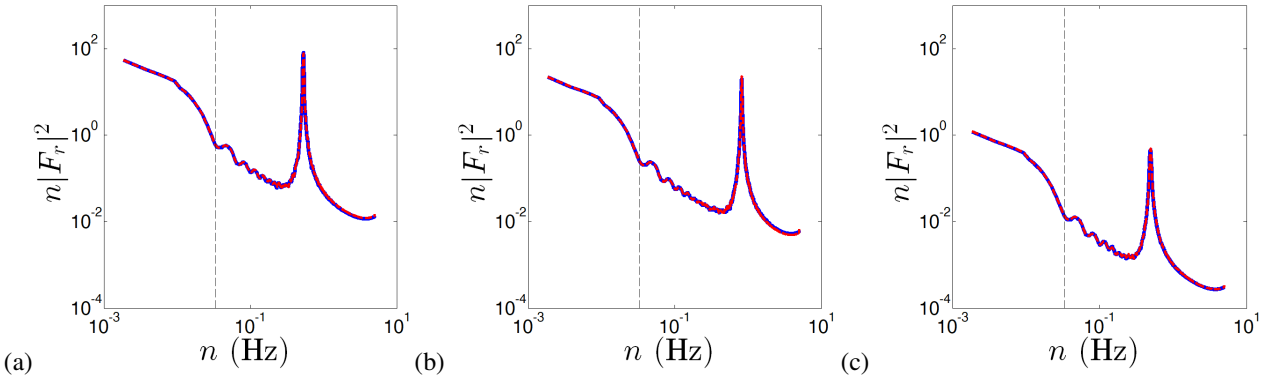

Fig. 11.

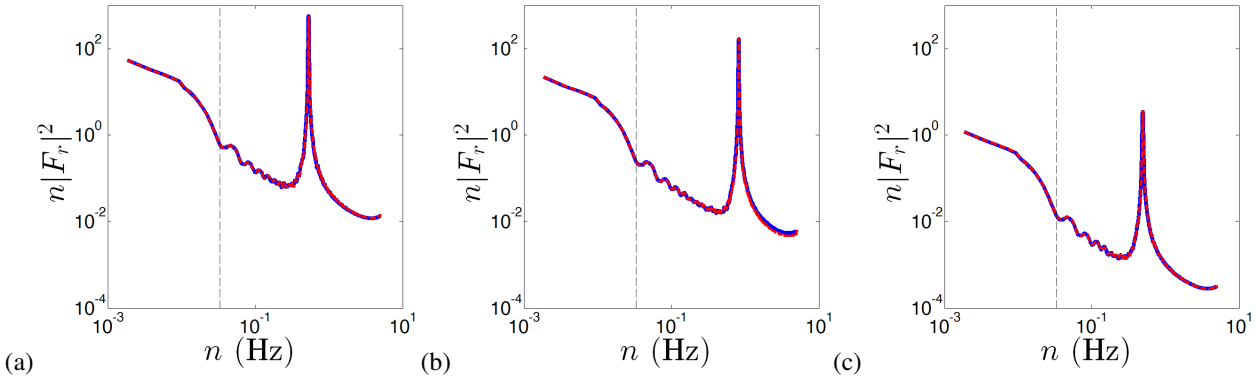

Fig. 12.

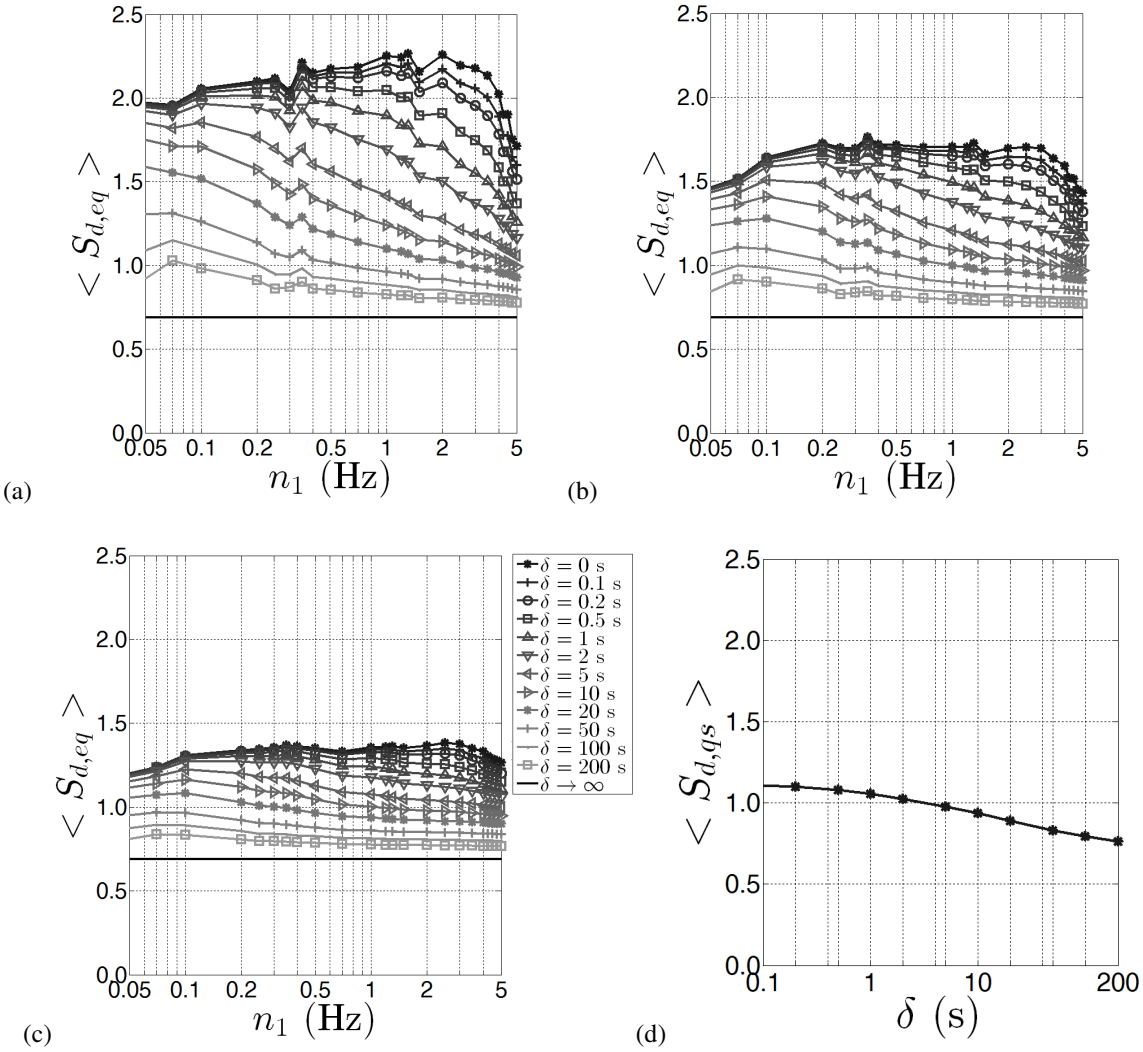
(a)
(b)
(c)
(d)
$< S_{d,eq} >$
n_1 (Hz)
δ (s)
$< S_{d,qs} >$
$\delta = 0$ s
$\delta = 0.1$ s
$\delta = 0.2$ s
$\delta = 0.5$ s
$\delta = 1$ s
$\delta = 2$ s
$\delta = 5$ s
$\delta = 10$ s
$\delta = 20$ s
$\delta = 50$ s
$\delta = 100$ s
$\delta = 200$ s
$\delta \to \infty$

Fig. 13.

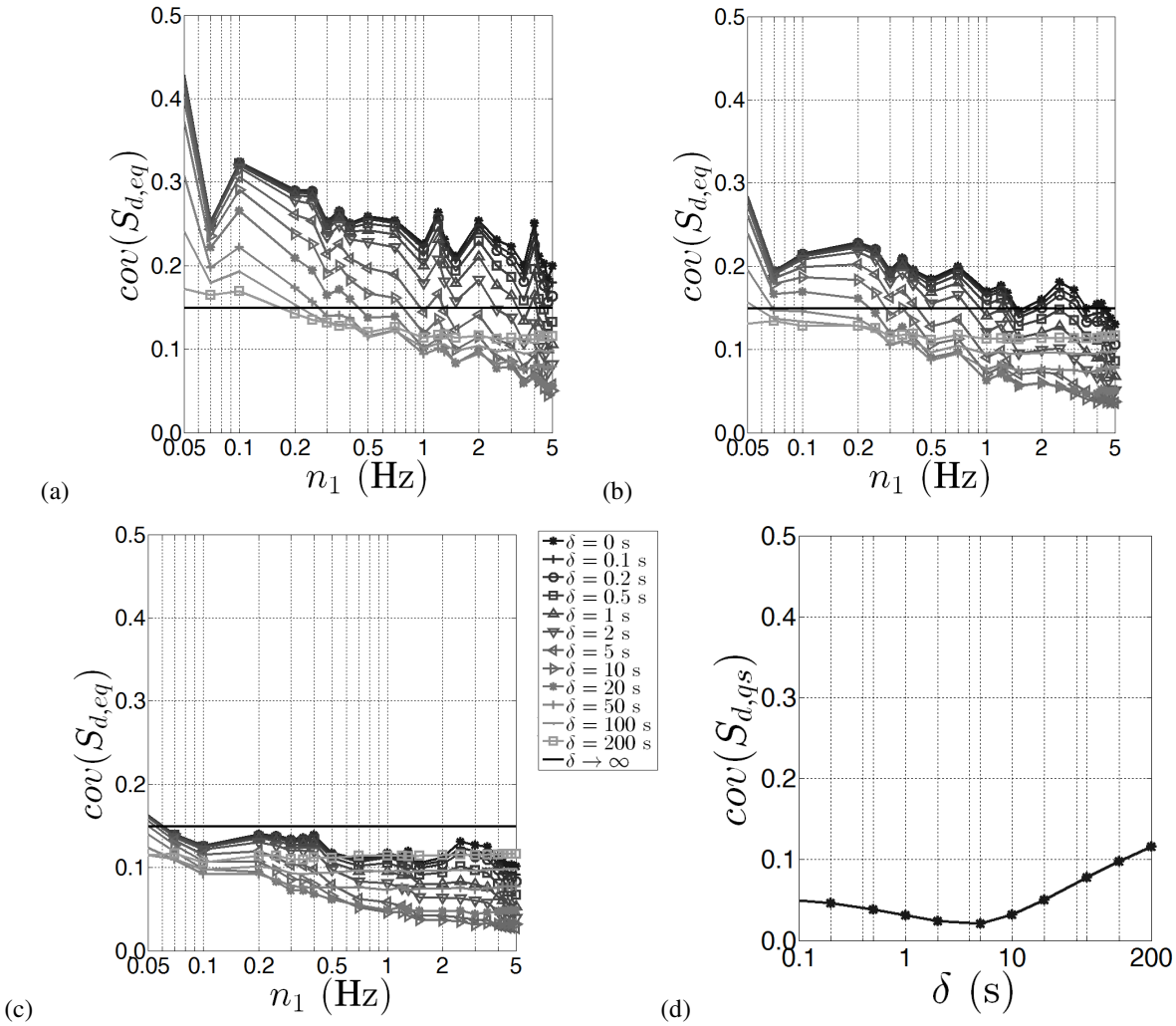
(a)
(b)
(c)
(d)
$cov(S_{d,eq})$
n_1 (Hz)
$cov(S_{d,qs})$
δ (s)
$\delta = 0$ s
$\delta = 0.1$ s
$\delta = 0.2$ s
$\delta = 0.5$ s
$\delta = 1$ s
$\delta = 2$ s
$\delta = 5$ s
$\delta = 10$ s
$\delta = 20$ s
$\delta = 50$ s
$\delta = 100$ s
$\delta = 200$ s
$\delta \to \infty$

Fig. 14.

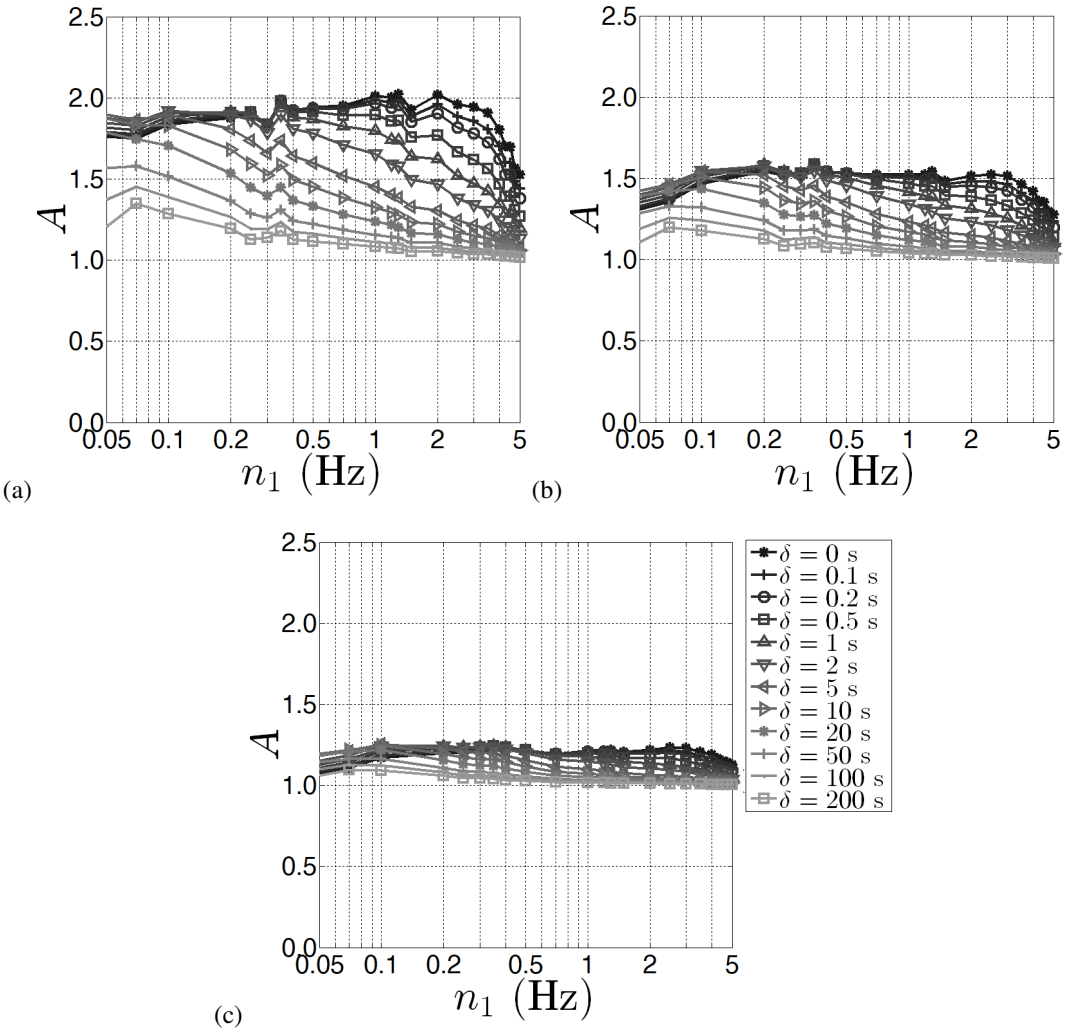
2.5
2.0
1.5
1.0
0.5
0.0
A
0.05 0.1 0.2 0.5 1 2 5
n_1 (Hz)
(a)
(b)
(c)
$\delta = 0$ s
$\delta = 0.1$ s
$\delta = 0.2$ s
$\delta = 0.5$ s
$\delta = 1$ s
$\delta = 2$ s
$\delta = 5$ s
$\delta = 10$ s
$\delta = 20$ s
$\delta = 50$ s
$\delta = 100$ s
$\delta = 200$ s

Fig. 15.

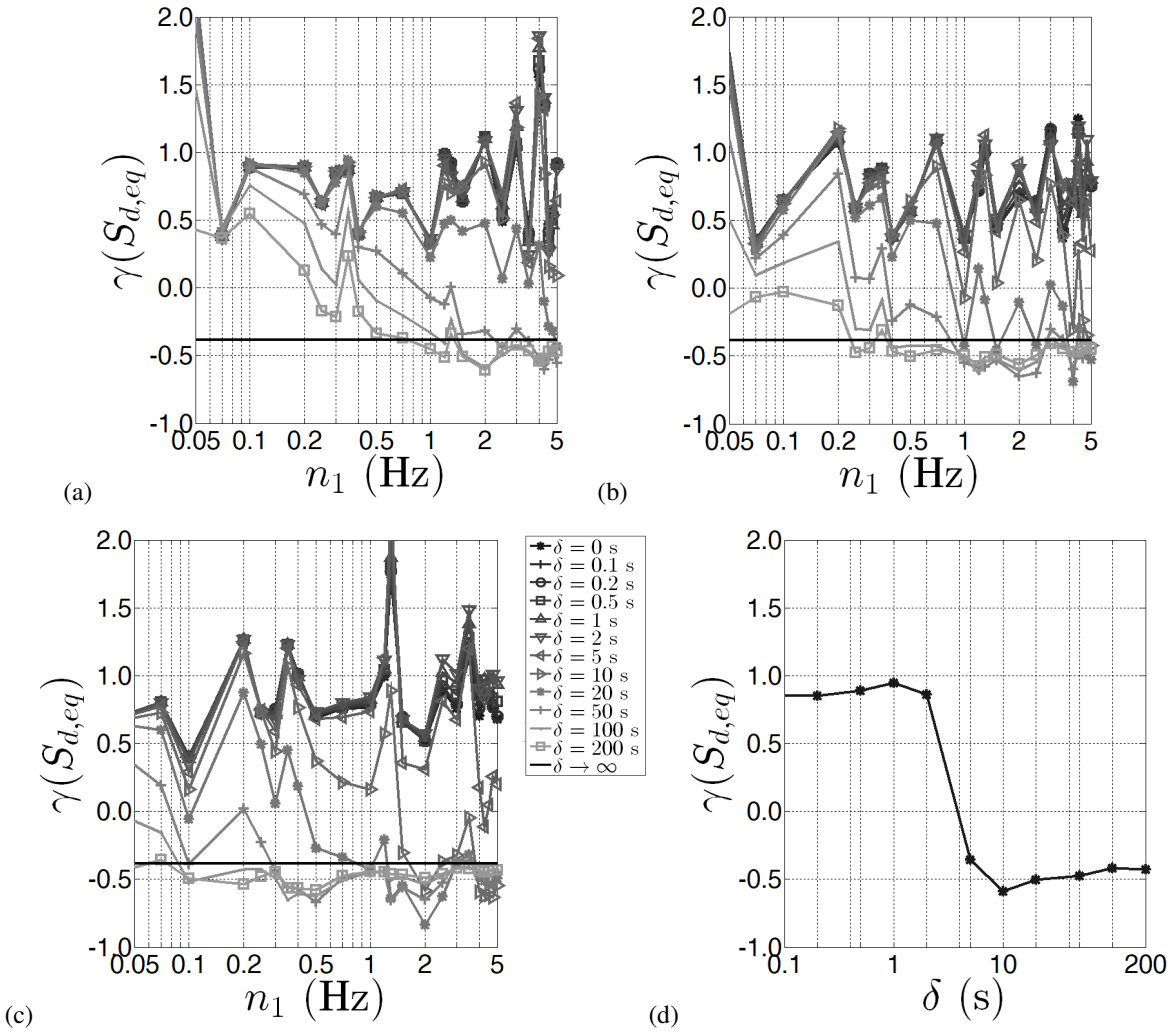
(a)
(b)
(c)
(d)
$\gamma(S_{d,eq})$
n_1 (Hz)
δ (s)
$\delta = 0$ s
$\delta = 0.1$ s
$\delta = 0.2$ s
$\delta = 0.5$ s
$\delta = 1$ s
$\delta = 2$ s
$\delta = 5$ s
$\delta = 10$ s
$\delta = 20$ s
$\delta = 50$ s
$\delta = 100$ s
$\delta = 200$ s
$\delta \to \infty$

Fig. 16.

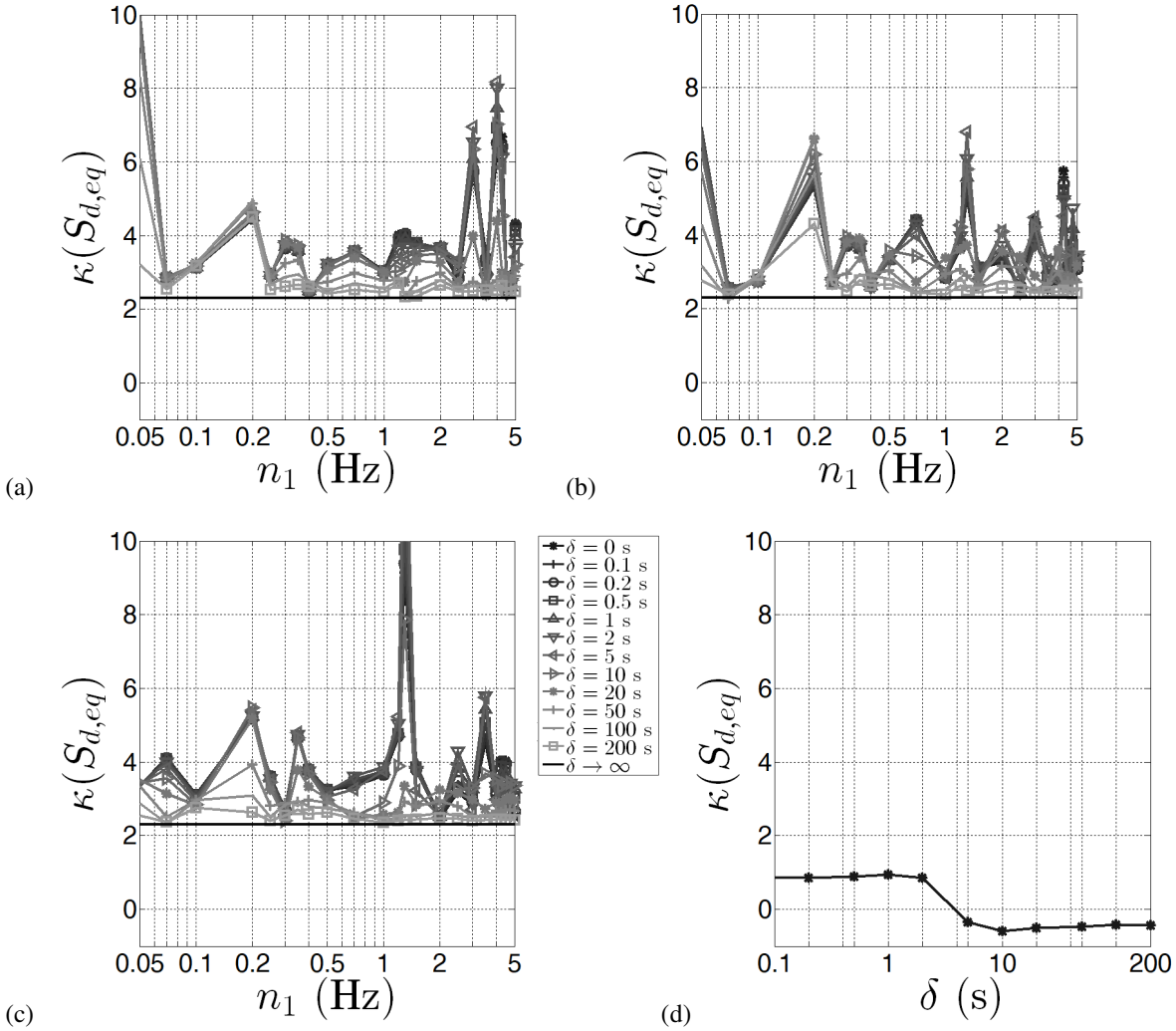
(a)
(b)
(c)
(d)
$\kappa(S_{d,eq})$
n_1 (Hz)
δ (s)
$\delta = 0$ s
$\delta = 0.1$ s
$\delta = 0.2$ s
$\delta = 0.5$ s
$\delta = 1$ s
$\delta = 2$ s
$\delta = 5$ s
$\delta = 10$ s
$\delta = 20$ s
$\delta = 50$ s
$\delta = 100$ s
$\delta = 200$ s
$\delta \to \infty$

Fig. 17.

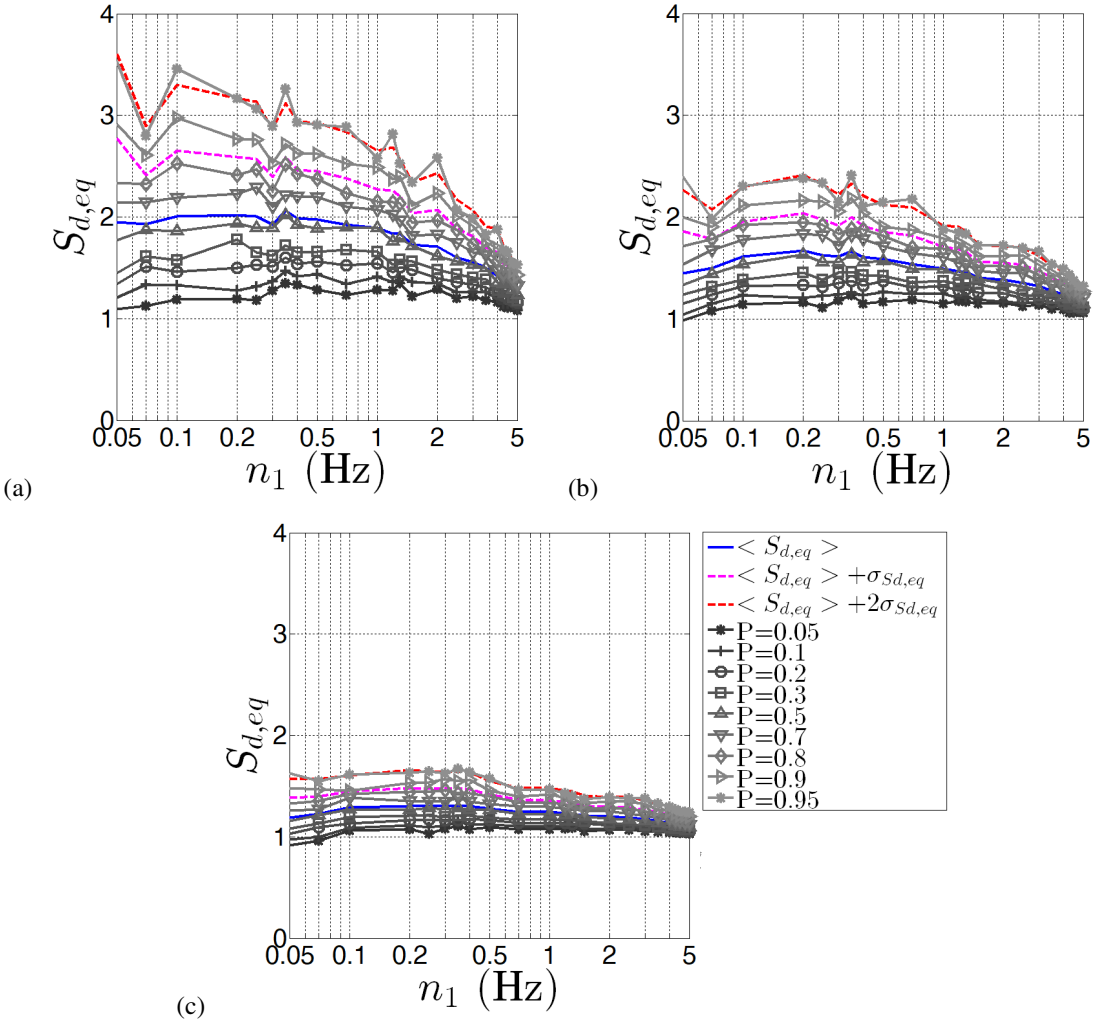
(a)
(b)
(c)
$S_{d,eq}$
n_1 (Hz)
0.05 0.1 0.2 0.5 1 2 5
0 1 2 3 4
$< S_{d,eq} >$
$< S_{d,eq} > +\sigma_{Sd,eq}$
$< S_{d,eq} > +2\sigma_{Sd,eq}$
P=0.05
P=0.1
P=0.2
P=0.3
P=0.5
P=0.7
P=0.8
P=0.9
P=0.95

Fig. 18.

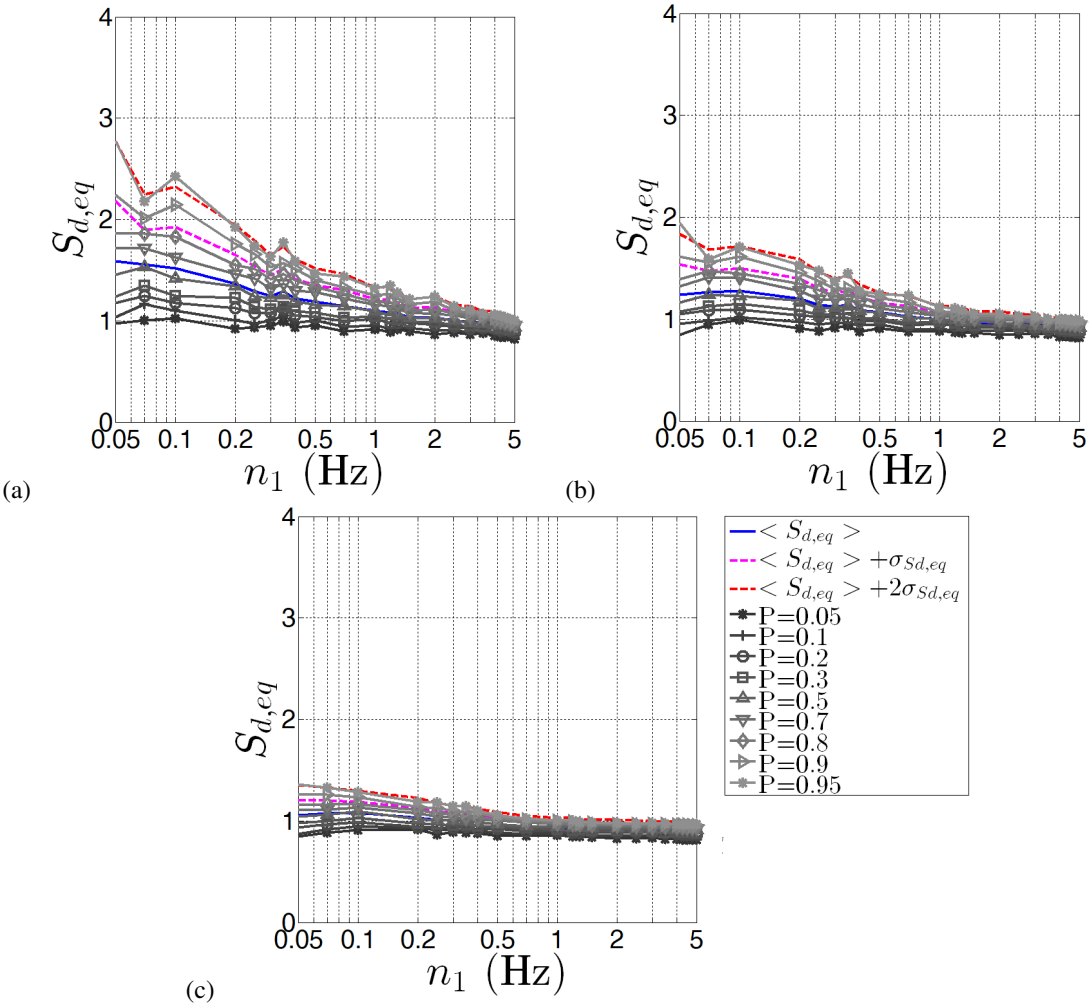
(a)
(b)
(c)
$S_{d,eq}$
n_1 (Hz)
0.05 0.1 0.2 0.5 1 2 5
0 1 2 3 4
$< S_{d,eq} >$
$< S_{d,eq} > +\sigma_{Sd,eq}$
$< S_{d,eq} > +2\sigma_{Sd,eq}$
P=0.05
P=0.1
P=0.2
P=0.3
P=0.5
P=0.7
P=0.8
P=0.9
P=0.95

Fig. 19.

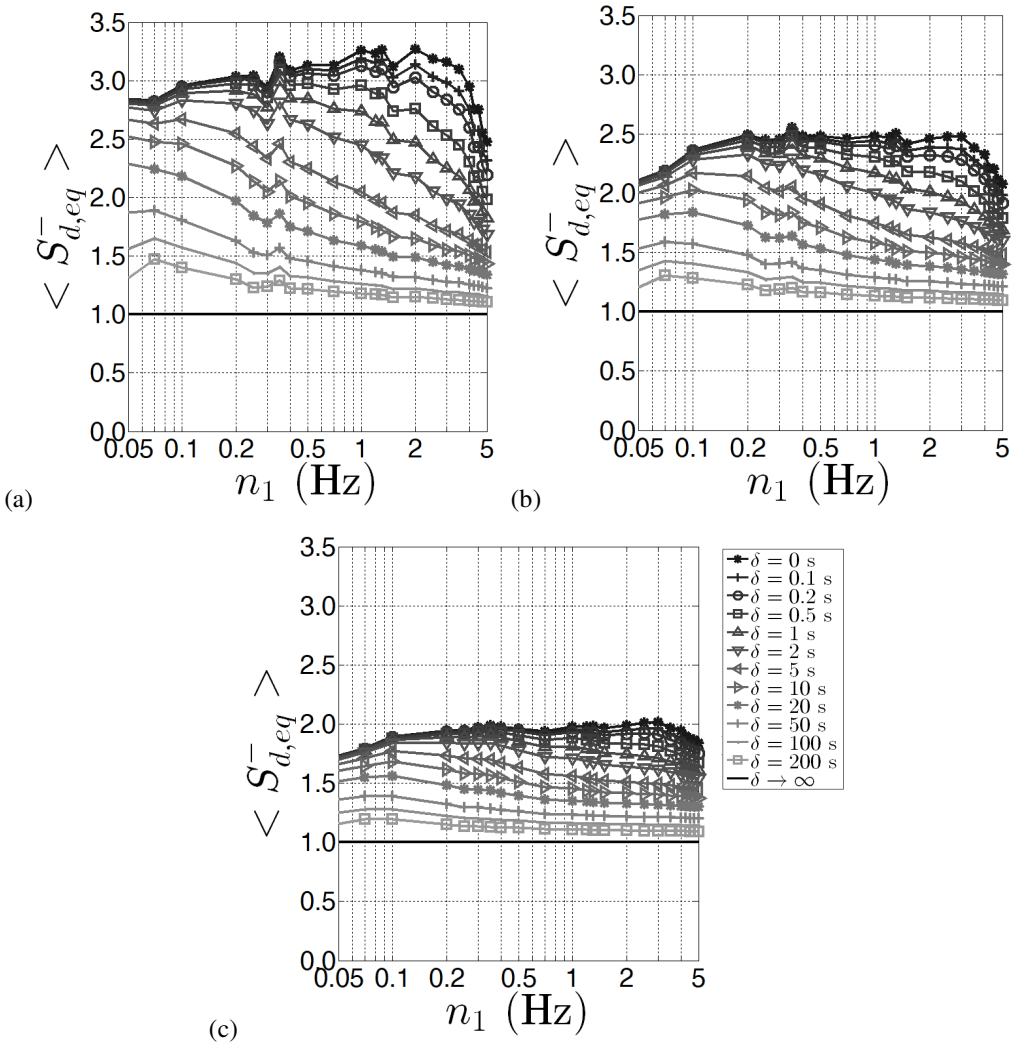
(a)
(b)
(c)
$< S^-_{d,eq} >$
n_1 (Hz)
0.05 0.1 0.2 0.5 1 2 5
0.0 0.5 1.0 1.5 2.0 2.5 3.0 3.5
$\delta = 0$ s
$\delta = 0.1$ s
$\delta = 0.2$ s
$\delta = 0.5$ s
$\delta = 1$ s
$\delta = 2$ s
$\delta = 5$ s
$\delta = 10$ s
$\delta = 20$ s
$\delta = 50$ s
$\delta = 100$ s
$\delta = 200$ s
$\delta \to \infty$

Fig. 20.

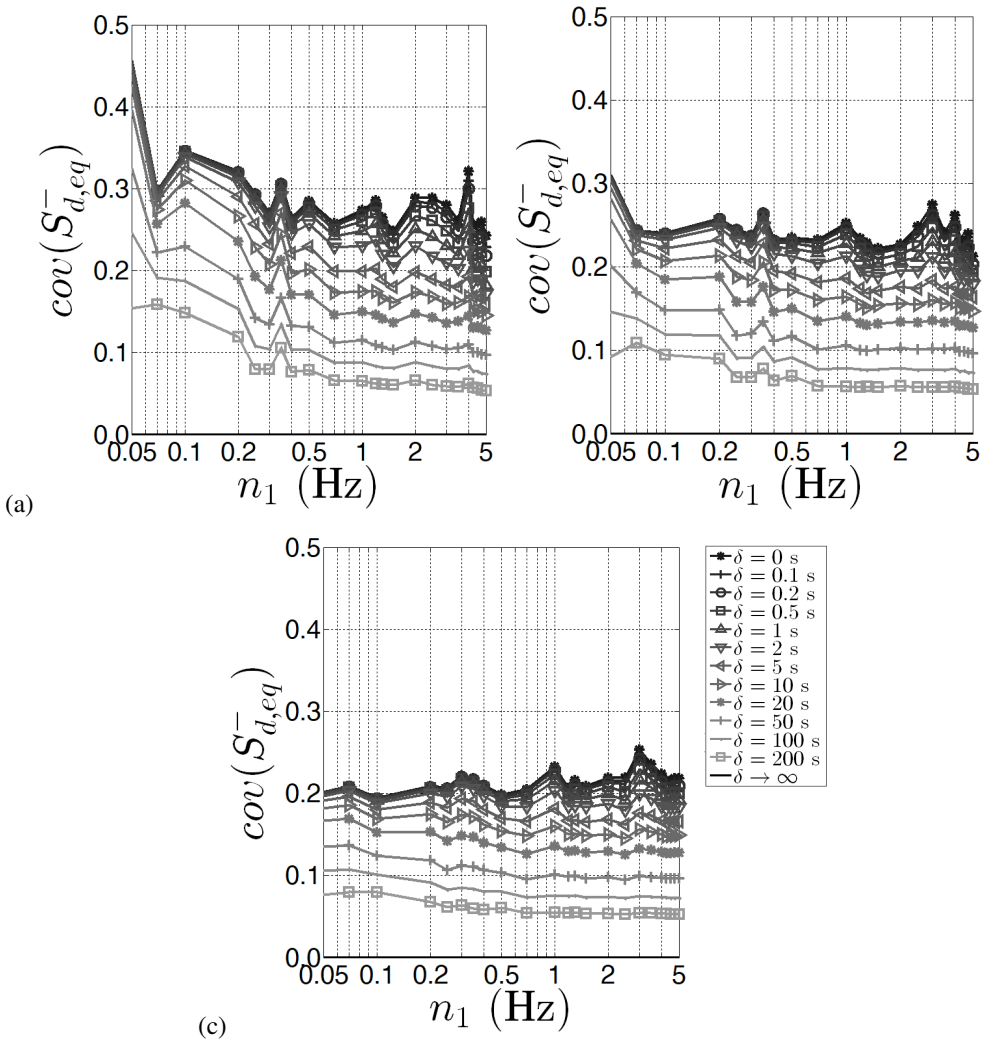
(a)
(c)
$cov(S^-_{d,eq})$
n_1 (Hz)
0.05 0.1 0.2 0.5 1 2 5
0.0 0.1 0.2 0.3 0.4 0.5
$\delta = 0$ s
$\delta = 0.1$ s
$\delta = 0.2$ s
$\delta = 0.5$ s
$\delta = 1$ s
$\delta = 2$ s
$\delta = 5$ s
$\delta = 10$ s
$\delta = 20$ s
$\delta = 50$ s
$\delta = 100$ s
$\delta = 200$ s
$\delta \to \infty$

Fig. 21.